ALMA MATER STUDIORUM

Università degli Studi di Bologna

Facoltà di Scienze Matematiche Fisiche e Naturali

Dottorato di Ricerca in Geofisica – XX Ciclo

Settore scientifico disciplinare: GEO/10

A comprehensive study of the 26^{th} December 2004 Sumatra earthquake: possible implications on Earth rotation and investigations on the coseismic and postseismic stress diffusion associated with the seismic rupture

Ph.D. Thesis of:

Anna Rita Pisani

Tutor: Dr. Antonio Piersanti

Supervisor: Prof. Maurizio Bonafede

Coordinator: Prof. Michele Dragoni

2008

ALMA MATER STUDIORUM

Università degli Studi di Bologna

Facoltà di Scienze Matematiche Fisiche e Naturali

Dottorato di Ricerca in Geofisica – XX Ciclo

Settore scientifico disciplinare: GEO/10

A comprehensive study of the 26^{th} December 2004 Sumatra earthquake: possible implications on Earth rotation and investigations on the coseismic and postseismic stress diffusion associated with the seismic rupture

Ph.D. Thesis of:

Anna Rita Pisani

Tutor: Dr. Antonio Piersanti

Supervisor: Prof. Maurizio Bonafede

Coordinator: Prof. Michele Dragoni

2008

Dedicated to

my husband

Acknowledgments

It is my pleasure to thank all the persons which contributed to this work of thesis. I am grateful to Dr. Piersanti who gave me the opportunity to do my Ph.D. studies in his group of research, for being my guide and mentor and his precious teachings.

I would like to thank Dr. Melini who introduced me to the group and assisted me constantly during these years.

I cannot forget all the researchers with which I had the possibility to collaborate during these three years and from which I received a scientific support, among them the Dr.ssa Volpe, Dr.ssa Cannelli, Dr. Casarotti and Dr. Devoti.

My special thanks go to my husband that with love, wisdom and patience encourages me to continue my career in the research world.

Contents

Abstract

In this work a multidisciplinary study of the December 26^{th}, 2004 Sumatra earthquake has been carried out. We have investigated both the effect of the earthquake on the Earth rotation and the stress field variations associated with the seismic event.

In the first part of the work we have quantified the effects of a water mass redistribution associated with the propagation of a tsunami wave on the Earth's pole path and on the length-of-day (LOD) and applied our modeling results to the tsunami following the 2004 giant Sumatra earthquake. We compared the result of our simulations on the instantaneous rotational axis variations with some preliminary instrumental evidences on the pole path perturbation (which has not been confirmed yet) registered just after the occurrence of the earthquake, which showed a step-like discontinuity that cannot be attributed to the effect of a seismic dislocation.

Our results show that the perturbation induced by the tsunami on the instantaneous rotational pole is characterized by a step-like discontinuity, which is compatible with the observations but its magnitude turns out to be almost one hundred times smaller than the detected one. The LOD variation induced by the water mass redistribution turns out to be not significant

because the total effect is smaller than current measurements uncertainties.

In the second part of this work of thesis we modeled the coseismic and postseismic stress evolution following the Sumatra earthquake. By means of a semi-analytical, viscoelastic, spherical model of global postseismic deformation and a numerical finite-element approach, we performed an analysis of the stress diffusion following the earthquake in the near and far field of the mainshock source. We evaluated the stress changes due to the Sumatra earthquake by projecting the Coulomb stress over the sequence of aftershocks taken from various catalogues in a time window spanning about two years and finally analyzed the spatio-temporal pattern.

The analysis performed with the semi-analytical and the finite-element modeling gives a complex picture of the stress diffusion, in the area under study, after the Sumatra earthquake. We believe that the results obtained with the analytical method suffer heavily for the restrictions imposed, on the hypocentral depths of the aftershocks, in order to obtain the convergence of the harmonic series of the stress components. On the contrary we imposed no constraints on the numerical method so we expect that the results obtained give a more realistic description of the stress variations pattern.

Chapter 1

Preface

The giant megathrust event occurred on the December 26^{th}, 2004 off the west coast of northern Sumatra, Indonesia, represents one of the most devastating earthquake of the modern history.

The oblique subducting motion of the Indo-Australian plate under the southeastern part of the Eurasian plate, segmented into Burma and Sunda subplates, ruptured a boundary of about 1300 km [Ammon et al., 2005]. The mainshock rupture began at 00:58:53 GMT at (3.3°N, 96.0°E) at a depth of about 30 km [Lay et al., 2005]; the Harvard Centroid Moment Tensor (CMT) solution indicates predominantly thrust faulting on a shallow dipping plane (8°) with a strike angle of 329°. The rake angle is 110° and indicates a slip direction $\sim 20°$ closer to the trench-normal direction than to the interplate convergence direction [Lay et al., 2005].

The CMT solution provided a scalar moment $M_0 = 3.95 \times 10^{22}$ Nm equivalent to a moment magnitude $M_w = 9.0$ [Dziewonski et al., 2000]. By studying the contribution of the very low frequency free oscillations, the

earthquake magnitude was estimated as $M_w = 9.3$, corresponding to a seismic moment of $M_0 = 1.0 \times 10^{23}$ Nm [Ammon et al., 2005, Park et al., 2005, Stein and Okal, 2005]. According to this estimate, the Sumatra event is the largest earthquake ever recorded after the 1960 Chile earthquake.

The undersea seismic rupture displaced a huge volume of water resulting in a tsunami wave that struck the coasts of the Indian Ocean causing massive damages and casualties. The 2004 tsunami is considered the deadliest in records.

The Sumatra earthquake represented a phenomenon that involved studies in many reaserch fields such us geophysics, geology, geodesy, etc., representing a unique opportunity to study, by means of new models and new technologies, the global effects of a giant seismic event on our Planet.

In this work, we were involved in a comprehensive study of the Sumatra earthquake, we evaluated the impact of the event on the secular pole motion and also the effects of the regional and long-distance stress transfer since the earthquake perturbed the stress field configuration over a wide area surrounding the mainshock source [Pollitz et al., 2006].

For decades researchers have aspired to predict the time and place of occurrence of disastrous shocks. Until the beginning of the 1990s, due the complexity of the seismogenetic faults, it was believed that large earthquakes occurred randomly and in unpredictable way, without influencing the timing or location of the next ones [Stein, 2003].

In the 2000s new studies showed that when an earthquake releases part of the stress accumulated in the Earth plate movements, there is a drop of the stress on the slipped fault and a raise of the stress elsewhere, at sites off the

slipped fault. The regions where the stress rises will be the sites where the next either large or small earthquakes will more likely occur. Even for small variations of stress, for exampe equal to one eighth of the pressure required to inflate a care tire, this process could be effective [Stein, 2003]. Infact as also reported in Stein [1999], the calculated off-fault stress increases rarely exceed few bars (1 bar = 0.1 MPa $\sim$ atmospheric pressure at sea level), or just a few percent of the mean earthquake stress drop. This hypothesis, known as stress triggering, continued to gain credibility due to the ability in explaining the location and frequency of earthquakes that followed several distructive shocks in California (Landers and Big Bear in 1992, Hector Mine in 1999) [Pollitz and Sacks, 2002] and in Turkey (Izmit and Düzce in 1999) [Parsons et al., 2000].

So, while evidences of fault interactions at local and regional scale were supported by several studies, the skepticism about the possibility to a interaction at long distances among seismogenetics structures [Kerr, 1998] began to be driven out starting from the work of Pollitz et al. [1998].

The occurrence of the giant Sumatra earthquake offers a chance to reopen the discussion about the fault interactions at local, regional and great distances from the event source by analyzing the coseismic and postsesimic stress pattern.

Within the realm of global effects, the Sumatra earthquake raised a big debate about its potential effect on Earth rotation. Earth scientists have tried to associate Earth rotational instabilities and seismic activity for 40 years. The attempts concerned both permanent instabilities, associated with global seismic activity as well as single detected irregularities in the pole

path, associated with single earthquakes [Soldati et al., 2001, Alfonsi et al., 1997, Dahlen, 1973, 1971].

The coseismic effects of the Sumatra earthquake affected many geophysical observables, among which the Earth rotation and gravitional field. In particular, a decrease of the LOD of 6.8 μs, a shift in the position of the mean rotation pole of 2.32 mas (milliarcseconds) towards 127° E longitude, a decrease of the Earth's oblateness J_2 of 2.37×10^{-11} and of the Earth's pear-shapedness J_3 of 0.63×10^{-11} [Gross and Chao, 2006, Boschi et al., 2006] are expected on the basis of current models; at the same time the accuracy of pole position detecting techniques have drastically improved in the last decades, yielding an increase in accuracy by more than two orders of magnitude since 1960.

These modeled coseismic effects on the Earth rotation are not evidenced by observations not even in the recent studies carried out by Gross and Chao [2006]; instead preliminary, but not still confirmed, observations in the geodetic measurements revealed a step-like discontinuity in correspondence of the Sumatra earthquake. A step-like shape, in agreement with the rotational theory, seemed to be not the footprint of a seismic event, being instead compatible with a transient effect.

The perspective to be involved in studies on such a relevant phenomenon, that for years scientist have tried to explain, motivated us to investigate the possible cause of such jump in the instantaneous rotational pole.

In this thesis, we treated separately the questions about the effect of the Sumatra event on the pole path and the stress diffusion due to the earthquake.

In the first chapter, on the basis of the standard rotational theory [Lam-

beck, 1980, Munk and MacDonald, 1960], we studied the perturbations to the instantaneous rotational pole by modeling an effect never investigated before, namely the effect due to the transient propagation of a tsunami wave both on the Earth pole path and on the length-of-day (LOD). We explained in details the theory that has been used to model such perturbation, we solved explicitly the excitation functions, which contain the perturbation, and the pole motion equations. Finally, the theory has been applied to the particular case of the tsunami wave that travelled along the Indian Ocean after the earthquake.

In the second chapter, we studied the stress field changes imposed by the Sumatra earthquake on the area along the Sunda (Java) Trench. This analysis has been performed taking advantage of a semi-analytical, viscoelastic, spherical model of global postseismic deformation developed by Piersanti et al. [1995] and a numerical finite-element approach developed by Volpe et al. [2007]. The Coulomb Failure Function variations, obtained by projecting the Coulomb stress on the sequence of the Sumatra aftershocks extracted from the USGS and CMT catalogue in a time window of two years after the event, helped us to evaluate how the stress due to the Sumatra earthquake acted to trigger the subsequent events.

Chapter 2

Effects of transient water mass redistribution associated with a tsunami wave on Earth's pole path

2.1 Introduction

Due to the action of various internal geophysical processes, the Earth rotates about an axis not aligned with its figure axis; this induces the Planet to wobble as it rotates. The Earth wobbles over a broad range of frequencies in response to a variety of forcing mechanisms; besides, it is characterized by a few discrete frequencies at which it naturally wobbles in the absence of forcing (this natural wobble is referred to as Chandler wobble) that are function of its internal structure. In absence of an excitation source, the Chandler

wobble would freely decay due to the action of dissipation processes, such as mantle anelasticity [Gross, 2003]. Since its discovery, several processes have been investigated to determine whether or not they could be excitation mechanisms of the Chandler wobble, for istance atmospheric processes, continental water storage cycles, core-mantle interactions and earthquakes (for a review, see Gross [2000] and references therein). The predominant mechanisms were found to be concerned with the periodical redistribution of atmospheric, oceanic and hydrologic masses [Gross, 2003].

In this part of the work, our aim is to study the perturbation to the instantaneous rotational pole due to a transient phenomenon that, to our knowledge, has not been still investigated: the transient water mass redistribution associated with the propagation of a tsunami wave.

Tsunamis are generally caused by seafloor perturbations associated mostly with earthquakes, submarine landslides or submarine volcanic eruptions. Not all earthquakes produce tsunamis because in order to generate them, they must occur at a shallow depth, have a large seismic moment and produce a significant vertical displacement of the sea floor.

In this chapter we are taking into account the propagation of a tsunami following a giant earthquake. The phenomenon involves both a permanent solid mass redistribution, represented by the static deformation induced by the earthquake and a transient water mass redistribution due to the tsunami propagation.

Such phenomenon, in agreement with the rotational theory, will be modeled by means of an excitation function that represents the forcing term in the pole motion equations.

Theoretically, the rotational effect on the pole path due to a seismic dislocation is a step-like perturbation that produces a jump of the excitation pole, while the instantaneous rotational pole describes a curve without breaks [Lambeck, 1980]. Such an effect on the Earth rotation has never been observed, not even in recent earthquakes (i.e. the 26th December 2004 Sumatra earthquake) [Gross and Chao, 2006], with the exception of a preliminary observation by Bianco et al. [2005a,b] who evidenced a step-like discontinuity in the pole path instead of the expected change in curvature radius in correspondence of the Sumatra earthquake.

The effect on the pole motion associated with a tsunami wave propagation is quite different from that produced by a permanent solid mass redistribution because it is the effect of a transient phenomenon due to the water mass redistribution. The rotational theory predicts that a transient phenomenon can be modeled by an excitation function with a delta-like temporal dependence that will give a step-discontinuous solution in the pole path [Lambeck, 1980], as it will be shown in section 2.2; the effect produced by such excitation could qualitatively explain the step-like discontinuity evidenced in Bianco et al. [2005a,b] data.

Using a synthetic numerical simulation of the 2004 Indian Ocean tsunami, we performed a forward modeling of the expected effect of the water mass transient redistribution on the pole path and length-of-day (LOD), that will be discussed in section 2.4. We explicitly computed the time dependent excitation functions, the pole path and the LOD variations induced by the tsunami wave. The pole path variations turn out to have the same temporal dependence of the step-like signal observed by Bianco et al. [2005a,b], but

their magnitude is too small to explain the observed data, besides the LOD variations turn out to be smaller than the uncertainty in the measurements.

2.2 Model formulation

The equations of motion for a deformable Earth come from the solution of the Liouville equation [Munk and MacDonald, 1960] and have the following form:

$$\dot{\mathbf{m}} = i\sigma_0(\mathbf{m} - \mathbf{\Psi}), \tag{2.1}$$

$$\dot{m}_3 = \dot{\Psi}_3 \tag{2.2}$$

where equation (2.1) describes the wobble, σ_0 is the frequency of the free oscillation (Chandler wobble) and $\mathbf{m} = m_1 + im_2$ represents the instantaneous rotational pole path in the complex plane. In equation (2.2) m_3 is related to the changes in the LOD ($\Delta\Lambda$) and to the instantaneous rotational velocity [Lambeck, 1980, Munk and MacDonald, 1960]; $\mathbf{\Psi} = \Psi_1 + i\Psi_2$ and Ψ_3 are the excitation functions which are used to describe, approximately, the phenomena which act to perturb the motion of the instantaneous rotational pole. $\mathbf{\Psi}$ represents the excitation pole, in the complex plane, around which revolves the instantaneous axis of rotation. Some examples of excitation functions useful to understand the phenomenon that we are going to study, will be given in subsection 2.2.1. In eqs. (2.1) and (2.2), $\mathbf{\Psi}$ and Ψ_3 represent the "modified excitation functions" which contain the perturbation associated with any prescribed event:

$$\boldsymbol{\Psi} = k_w \boldsymbol{\psi} \tag{2.3}$$

$$\Psi_3 = k_{LOD} \psi_3 \tag{2.4}$$

where $\boldsymbol{\psi} = \psi_1 + i\psi_2$ is a vector quantity and k_w and k_{LOD} are the "transfer functions" which arise from the correction for the elastic deformation associated with the centrifugal forces due to Earth rotation; their values depend on whether the event does or does not load (i.e. winds) the Earth [Lambeck, 1980, Munk and MacDonald, 1960]. The solutions of equation (2.1) for the wobble and of equation (2.2) for the LOD variations are:

$$\mathbf{m}(t) = \mathbf{m}_0 e^{i\sigma_0 t} - i\sigma_0 e^{i\sigma_0 t} \int_{-\infty}^{t} \boldsymbol{\Psi}(\tau) e^{-i\sigma_0 \tau} d\tau \tag{2.5}$$

$$\frac{\Delta\Lambda}{\Lambda_0} = \frac{\Omega - \omega_3}{\Omega} = -m_3 = -\Psi_3 \tag{2.6}$$

where $\mathbf{m_0}$ is an arbitrary complex constant, Λ_0 is the nominal LOD (e.g. 86400 s), Ω is the mean angular velocity of the Earth and ω_3 is the instantaneous rotational velocity [Lambeck, 1980, Munk and MacDonald, 1960]. In particular, once the excitation function $\boldsymbol{\Psi}$ has been determined, the effect of a perturbation to the istantaneous pole of rotation at any time t can be quantified from equation (2.5). In this case, since we are studying a perturbation occurring on a short time scale than the 14 months Chandler period, we will neglect the term of free nutation $\mathbf{m}_0 e^{i\sigma_0 t}$ and will solve the partial solution of the pole motion equation:

$$\mathbf{m}(t) \sim -i\sigma_0 e^{i\sigma_0 t} \int_{-\infty}^{t} \mathbf{\Psi}(\tau) e^{-i\sigma_0 \tau} d\tau \tag{2.7}$$

while the variation of the LOD can be directly obtained from eq. (2.6).

2.2.1 Solution of motion for simple excitation functions

Many of the geophysical phenomena perturbing the Earth rotation can be approximated by simple excitations such as step, delta, ramp or periodic functions. The ramp function represents an excitation that occurs if there is a secular exchange of mass between the polar ice caps and the oceans, while a periodic function is a useful model related to the electromagnetic core-mantle coupling mechanism [Lambeck, 1980].

As we explained in the introduction, in this chapter we are taking into account the propagation of a tsunami following a giant earthquake.

Since the phenomenon that we are going to study is concerned both with the earthquake that generates the tsunami and the propagation of the wave through the ocean, in this subsection, following the rotational theory, our aim is to give a schematic example of the effects produced by these phenomena on the Earth pole path.

Step excitation function

A step excitation function is the best representation of the effect due a permanent dislocation associated with a seismic event and has the following form:

$$\boldsymbol{\Psi}(t) = \boldsymbol{\Delta\Psi} H(t) \tag{2.8}$$

where

$$H(t) = \begin{cases} 0 & \text{for } t < 0 \\ 1 & \text{for } t > 0 \end{cases} \tag{2.9}$$

is $H(t)$ is the Heaviside step function and $\boldsymbol{\Delta\Psi}$ is the amplitude of the excitation; this excitation represents an instantaneous shift of the excitation pole at $t = 0$. In correspondence of this excitation, for $t \geq 0$, the partial solution of the instantaneous pole of rotation (2.7) becomes:

$$\begin{aligned} \mathbf{m}(t) &= -i\sigma_0 e^{i\sigma_0 t} \int_0^t \boldsymbol{\Delta\Psi} e^{-i\sigma_0 \tau} d\tau \\ &= \boldsymbol{\Delta\Psi}(1 - e^{i\sigma_0 t}). \end{aligned} \tag{2.10}$$

At the time $t = 0$ the excitation pole has jumped from $\boldsymbol{\Psi} = 0$ to a new position $\boldsymbol{\Psi} = \boldsymbol{\Delta\Psi}$ about which the rotation axis begins to turn. If there are other jumps for $t > 0$ from $\boldsymbol{\Delta\Psi}$ to $\boldsymbol{\Delta\Psi} + \boldsymbol{\Delta\Psi}'$ the instantaneous pole of rotation will begin to rotate around this new position describing a continuous curve with a sudden change in the curvature radius when the perturbation is "turned on" [Lambeck, 1980] (figure 2.1a).

The effect produced by such excitation on the Earth pole path is not compatible with the step-like discontinuity observed in the geodetic data of Bianco et al. [2005a,b].

Delta excitation function

An excitation represented by a sudden impulse is described by a Dirac delta function

$$\mathbf{\Psi}(t) = \mathbf{\Delta\Psi}\delta(t) \tag{2.11}$$

where

$$\begin{gathered}\delta(t) = 0, \text{for } t < 0 \text{ and for } t > 0 \\ \int_{-\infty}^{\infty} \delta(t)dt = 1 \\ \delta(t) = \int_{-\infty}^{t} \delta(t)dt \begin{cases} 0 & \text{for } t < 0 \\ 1 & \text{for } t > 0 \end{cases}\end{gathered} \tag{2.12}$$

In this case the partial solution of the wobble equation (2.7) becomes:

$$\begin{aligned}\mathbf{m}(t) &= -i\sigma_0 e^{i\sigma_0 t}\mathbf{\Delta\Psi} \int_{-\infty}^{t} \delta(\tau)e^{-i\sigma_0\tau}d\tau \\ &= \sigma_0 e^{i\sigma_0 t}\mathbf{\Delta\Psi}e^{-i(\sigma_0 t+\frac{\pi}{2})} \\ &= -i\sigma_0 e^{i\sigma_0 t}\mathbf{\Delta\Psi}H(t).\end{aligned} \tag{2.13}$$

In this case the excitation pole remains at its original position while the instantaneous rotational pole ω undergoes a jump of magnitude $\sigma_0\mathbf{\Delta\Psi}$ and is shifted $\frac{\pi}{2}$ from the direction of the impulse [Lambeck, 1980] (figure 2.1b).

A delta excitation function describes a perturbation compatible with tran-

sient phenomena such as the redistribution of water mass due to the propagation of a tsunami wave. Such excitation induce a jump in the Earth pole path compatible with that detected in the observations of Bianco et al. [2005a,b].

2.2.2 Tsunami excitation function

In order to estimate the perturbation to the istantaneous pole of rotation and to the LOD due to a transient water mass displacement occurred during the propagation of a tsunami, we have to calculate first the corresponding time dependent excitation functions.

The perturbation due to a propagation of a tsunami wave may be modeled with the excitation function $\mathbf{\Psi}_t$ expressed as the sum of two main contributions:

$$\mathbf{\Psi}_t{}^{(wobble)} = \mathbf{\Psi}_m + \mathbf{\Psi}_v \tag{2.14}$$

$$\Psi_t{}^{(LOD)} = \Psi_m + \Psi_v \tag{2.15}$$

where the temporal dependence has been left implicit for the sake of clarity. $\mathbf{\Psi}_m$ and Ψ_m are associated with the perturbation to the Earth static mass distribution caused by the variation of the sea surface ("matter" term); in this case the event loads the Earth, so the transfer functions in eq. (2.3) and in eq. (2.4) assume the following values $k_w = 1.03$ and $k_{LOD} = 0.7$ [Lambeck, 1980, Munk and MacDonald, 1960]. $\mathbf{\Psi}_v$ and Ψ_v are associated with the angular momentum exchange between the horizontal flowing water and the solid Earth ("velocity" term); in this case there is no loading so the

transfer functions in eq. (2.3) and in eq. (2.4) assume the following values $k_w = 1.47$ and $k_{LOD} = 1.0$ [Lambeck, 1980, Munk and MacDonald, 1960]. Therefore the total excitation functions for the perturbation to the pole path in eq. (2.7) and to the LOD in eq. (2.6) can be written as follows:

$$\boldsymbol{\Psi}_t{}^{(wobble)} = 1.03\boldsymbol{\psi}_m{}^{(wobble)} + 1.47\boldsymbol{\psi}_v{}^{(wobble)} \tag{2.16}$$

$$\Psi_t{}^{(LOD)} = 0.7\psi_m{}^{(LOD)} + \psi_v{}^{(LOD)} \tag{2.17}$$

where $\boldsymbol{\psi}_m$ and $\boldsymbol{\psi}_v$ are vector quantities. In spherical coordinates the excitation functions corresponding to a water mass element $dm = \rho_w dV$ located at latitude θ and longitude ϕ read ("matter" term) [Lambeck, 1980]:

$$\begin{pmatrix} \psi_1 \\ \psi_2 \end{pmatrix}_m^{(wobble)} = -\int_{V_w} \frac{\rho_w}{C-A} r^2 \cos\theta \sin\theta \begin{pmatrix} \cos\phi \\ \sin\phi \end{pmatrix} dV \tag{2.18}$$

$$\psi_m{}^{(LOD)} = -\int_{V_w} \frac{\rho_w}{C} r^2 \cos^2\theta \; dV \tag{2.19}$$

where the integration is carried out over the wave volume V_w that grows up above the unperturbed sea surface, while C and A are the axial and the equatorial inertia moment of the Earth.

The excitation functions corresponding to a mass $dm = \rho_w dV$ moving with tangential velocity $\mathbf{v} = (v_\theta, v_\phi)$ read ("velocity" term) [Lambeck, 1980]:

$$\begin{pmatrix} \psi_1 \\ \psi_2 \end{pmatrix}_v^{(wobble)} = \int_{V_o} \frac{2\rho_w}{\Omega\,(C-A)} r v_\phi \sin\theta \begin{pmatrix} -\cos\phi \\ -\sin\phi \end{pmatrix} dV + \\ + \int_{V_o} \frac{2\rho_w}{\Omega\,(C-A)} r v_\theta \sin^2\theta \begin{pmatrix} \sin\phi \\ -\cos\phi \end{pmatrix} dV \qquad (2.20)$$

$$\psi_v{}^{(LOD)} = -\int_{V_o} \frac{\rho_w}{\Omega C} r v_\phi \cos\theta \; dV \qquad (2.21)$$

where Ω is the mean Earth angular velocity and V_0 is the total oceanic volume involved in the tsunami propagation evaluated considering the volume of water under an unperturbed oceanic surface.

The excitation functions resulting from the integration of eqs. (2.18)-(2.19) and (2.20)-(2.21) will represent by construction a transient phenomenon: in fact the wave volume V_w in eqs. (2.18)-(2.19) and the velocity fields in eqs. (2.20)-(2.21) are identically null before and after the tsunami propagation, so that the excitation functions will be non-zero only during the tsunami propagation.

To evaluate the "matter" and "velocity" terms of the excitation functions (2.18)-(2.19) and (2.20)-(2.21) we estimated the water vertical displacement and the horizontal velocity, as a function of time, by means of a numerical tsunami model [Mader, 2004, Mei, 1983], in the whole area interested by the propagation of the tsunami.

Once the sea depth $h(\theta, \phi)$, the water elevation $z(\theta, \phi)$ and the horizontal velocity vector $\mathbf{v}(\theta, \phi)$ have been determined, the excitation functions can be

obtained through a numerical integration by substituting

$$dV = z(\theta, \phi) r^2 \cos\theta d\theta d\phi$$

in eqs. (2.18)-(2.19) and

$$dV = [h(\theta, \phi) + z(\theta, \phi)] r^2 \cos\theta d\theta d\phi \simeq h(\theta, \phi) r^2 \cos\theta d\theta d\phi$$

in eqs. (2.20)-(2.21). The last two integrations have been carried out dropping z, under the assumption $z << h$. This approximation is adequate everywhere in the domain in which we performed our simulations, with the exception of the proximity of the coasts, where anyway the contribution to the integration of the eqs. (2.20)-(2.21) results to be negligible.

Afterwards, the variation in the pole path can be computed by numerically integrating eq. (2.7) while the LOD variation is directly obtained from eq. (2.6).

2.3 The tsunami modeling

Tsunamis propagate in the sea as gravity waves and since their wavelength (typically of the order of $\sim 10^4 - 10^5 m$) is at least one order of magnitude larger than the sea depth ($< 10^3 m$), they are considered as long waves propagating in shallow waters [Piatanesi and Tinti, 1998]. In open water tsunamis have extremely long periods (from minutes to hours) and travel across the ocean with typical speeds from 500 to 1000 km/h and with a phase velocity given by $c = \frac{\lambda}{\tau} = \sqrt{gh}$, where g is the gravity acceleration and h is the sea

depth; so when the wave approaches the coast and the sea depth becomes small the wave velocity diminishes and, in agreement with the Green's law, the front wave grows up as $a = h^{-\frac{1}{4}}$, where a is the amplitude of the wave and h is the sea depth [Lamb, 1932]. During the propagation the waves have a little energy loss even over long distances and their motion involve the entire water column from the surface to the sea bed. The tsunamis are very different from typical wind-generated waves in the ocean, which have typical periods of about 10 s and wavelengths of 150 m with a motion that typically involves only a zone down to a depth of few tens of meters.

The model for tsunami propagation is based on the nonlinear nondispersive shallow-water approximation of the Navier-Stokes equations which describe the evolution of an incompressible fluid in response to gravitational and rotational accelerations (e.g. Piatanesi and Tinti [1998]). In the classical theory of shallow water, the vertical component of the water particles is assumed negligible [Mader, 2004, Lautrup, 2005] and the horizontal velocity field is retrieved from the mass and momentum equations:

$$\frac{\partial (z+h)}{\partial t} + \nabla \cdot (\mathbf{v}\,(z+h)) = 0 \tag{2.1}$$

$$\frac{\partial \mathbf{v}}{\partial t} + (\mathbf{v} \cdot \nabla)\,\mathbf{v} = g\nabla z + \mathbf{C} \tag{2.2}$$

where z is the water elevation above the unperturbed sea level, $\mathbf{v}$ is the depth-averaged horizontal velocity vector, h is the sea depth, g is the gravity acceleration and $\mathbf{C}$ represents the Coriolis force; the frictional term has been neglected from the eq. (2.2) because we deal with a propagation of a

wave in deep waters (transoceanic). This system is completed by boundary conditions of pure wave reflection along the coastlines and of full wave transmission at the open ocean. We assume that the initial tsunami wave is set in motion by the instantaneous transmission of the sea bed displacement to the overlying water mass. Once the seismic fault geometry has been specified, we compute the coseismic deformation of the sea floor using an elastic dislocation model [Okada, 1985]. Equations (2.1) and (2.2) are solved numerically by means of a finite difference method in a staggered grid of 2 arcminutes of spatial resolution [Mader, 2004, Mei, 1983].

2.4 Application to the Sumatra event

In this section our aim is to study the effect of the transient water mass redistribution on the pole path applying the theoretical model, developed above, to the tsunami wave following the devastating megathrust earthquake of December 26, 2004 off the west coast of northern Sumatra.

The Sumatra event has been considered the largest after the 1960 Chile earthquake and reopened discussions and stimulated investigations on the possible effects of earthquakes on the Earth rotation.

In recent studies Gross and Chao [2006] modeled the expected coseimic effects on the Earth rotation due to the Sumatra earthquake, obtaining a shift of the excitation pole of 2.32 mas and a LOD decrease of 6.8 μs. Since the polar motion excitation functions and the LOD can currently be determined with an accuracy of 5 mas and 20 μs, respectively, these changes in the Earth rotation turn out to be about three times smaller than the measure-

ments uncertainties. Moreover the analysis performed on the Earth rotation observations do not show evidence of a signal induced by the Sumatra earthquake [Gross and Chao, 2006].

Otherwise preliminary geodetic observations of Bianco et al. [2005a,b], based on laser ranging and GPS techniques, reveal a westward step discontinuity in the y-pole component of the instantaneous rotational pole path in correspondence of the earthquake, as it is shown in figures 2.2 and 2.3. The observed discontinuity, however, has not been confirmed but, in our opinion, is an evidence which is worth considering.

Figure 2.2 shows the observed discontinuity in the SLR data. The analysis, based on the extimates of the residuals of the quadratic polinomial fit of the y-pole component data, revealed a jump of magnitude of about $1.5 - 2.0$ mas. Figure 2.3 shows a work, performed some months later, in which different analyses, retrieved by means different geodetic techniques, evidence coherently the step discontinuity in correspondence of the Sumatra event.

Theoretically, the observed step-like discontinuity cannot be explained only in terms of a solid mass redistribution associated with a coseismic permanent dislocation. As discussed in subsection 2.2.1, a step-like discontinuity in the pole path may be modeled with an excitation having a delta-like temporal dependence, which represents a transient perturbation induced, for istance, by a tsunami wave propagation.

Since the time scale in which we perform our analysis (i.e. 16 hours) is less than that the pole path determination (i.e. about 24 hours) we expect that the functional form of excitation associated with the propagation of the tsunami wave, shows a delta-like temporal dependence which represents a

step-like discontinuity in the pole path.

The time dependent excitation functions have been evaluated by means of a numerical tsunami model, whose outputs are the vertical displacement and the horizontal velocity field of the propagating tsunami wave, as described in section 2.3. The numerical tsunami simulation has been carried out in a time window of 16 hours (i.e. 57600 s) and on a spatial domain covering the whole Indian Ocean area interested by the propagation of the tsunami (about 10^8 km^2). The tsunami source geometry is the one obtained by Bao et al. [2005] and summarized in the table of figure 2.4.

The volume V_0 on which the integration of eq. (2.20) and eq. (2.21) has been carried out takes into account the Indian Ocean bathymetry from the ETOPO2 dataset [Smith and Sandwell, 1997] available at http://www.ngdc.noaa.gov/mgg/global/global.html.

Figure 2.5 shows the snapshots of the elevation and velocity fields of the modeled tsunami, taken at 4 hours interval. The bathymetric complexities of the Indian Ocean, such as trenches, ridges and seamounts, affect the tsunami propagation and induce strong refraction of the wavefields. In the open sea, the tsunami waves hardly exceed an amplitude of 10 cm while the induced particle velocity is generally smaller than 1 mm/s. On the contrary, due to the conservation of the quantity of motion, when the waves enter in very shallow waters and approach the coastline, the water elevation may grow up to several meters and the velocity may be as large as few m/s.

The temporal evolution of the Ψ_1 and Ψ_2 components and of $|\boldsymbol{\Psi}_t|$ are reported in figure 2.6 and 2.7. Figure 2.7 shows that the maximum variation of $\boldsymbol{\Psi}_t$ during the propagation of the tsunami wave exceeds 2×10^{-8}. The

curves plotted between the dotted lines evidence the delta-like temporal evolution of the perturbation associated with the simulated tsunami, out of the simulated range the curves have been smoothly cut off in order to mimic an excitation that "turns on" and "switches off". If we compare our result to those obtained for the coseismic effect of the Sumatra earthquake by Gross et al. (2006) it can be seen that this value is two times greater than the one associated with the seismic excitation function $\mathbf{\Psi}_e$ that has been estimated to be about 10^{-8}. This of course does not imply that the pole path perturbation induced by the tsunami is more significant, due to the different temporal dependence between $\mathbf{\Psi}_e$ and $\mathbf{\Psi}_t$.

From the numerical integration of eq. (2.7) we obtained the temporal evolution of the pole position shown in figure 2.8. Figure 2.9 shows the evolution of the instantaneous pole of rotation (polodia) during the 16 hours of simulation of the tsunami. As can be seen from figure 2.8, the propagation of the tsunami wave induces a step-like perturbation in the pole path with a magnitude of about 0.02 mas.

According to what we obtained the observed step-like discontinuity of figures 2.2 and 2.3 could be related to an excitation with a delta-like temporal dependence due to transient mechanisms. We compared our modeled step discontinuity with that observed in geodetic data and even if the curves have the same temporal dependence, our result is almost one hundred times smaller than the observed, therefore too small to be detectable.

Figure 2.10 shows the evolution of LOD variations during the propagation of the simulated tsunami obtained from eq. (2.6). The plot evidences a transient perturbation of LOD in agreement with the transient nature of a

water mass redistribution. The transient corresponds to a LOD decrease as in the case of static coseismic deformation and has a peak of 8.8 μs four hours after the beginning of the tsunami propagation, greater than the value obtained by Gross and Chao [2006] as a result of solid mass redistribution (6.8 μs).

Anyway, these transient variations occur in a too short time window to be evidenced by the current daily measurement techniques. We note also that, since the LOD changes can currently be determined with an accuracy of about 20 μs [Gross and Chao, 2006] and our modeled LOD variations are 2.3 times smaller than the uncertainty in the measurements, the changes due to a water mass redistribution could be too small to be detected.

2.5 Conclusions

In this chaper we studied the effect of a perturbation to the Earth rotation due to a transient phenomenon associated with the propagation of a tsunami wave that has been never investigated yet.

We developed a theoretical model to evaluate the effect of a transient water mass redistribution on the instantaneous pole of rotation and on the LOD. The modeling is based on the explicit solution of the partial pole motion equation that can be retrieved by means of the calculation of the excitation functions, according with the theory outlined in Lambeck [1980] and Munk and MacDonald [1960], which contain the perturbation to the pole path and to the LOD. Since the perturbation is associated both with the redistribution of mass caused by the variation of sea surface and the

exchange of angular momentum between the solid Earth and the horizontal flowing water, a numerical tsunami model has been used to evaluate the vertical displacement of the wave and the horizontal velocity field.

The effect of such perturbation on the Earth pole path has been evaluated by applying the modeling scheme to the tsunami following the Sumatra earthquake.

The effect produced by the modeled water mass redistribution on the pole path is qualitatively in agreement with the observed step-like discontinuity in the pole path but its magnitude is one hundred times smaller than that assessed in geodetic data. The geodetic observations however have still to be confirmed, but unfortunately no work on this topic is available in the literature yet.

The LOD variation caused by the modeled tsunami is a transient decrease with a peak value greater than the coseismic effect due to the static dislocation, but its time scale is too short to be detected by current measurement techniques and its amplitude is smaller than current measurement uncertainties.

Therefore we have to discard the perturbation effect of the tsunami as a possible explanation of the step-like discontinuity in the pole path observed in available geodetic data.

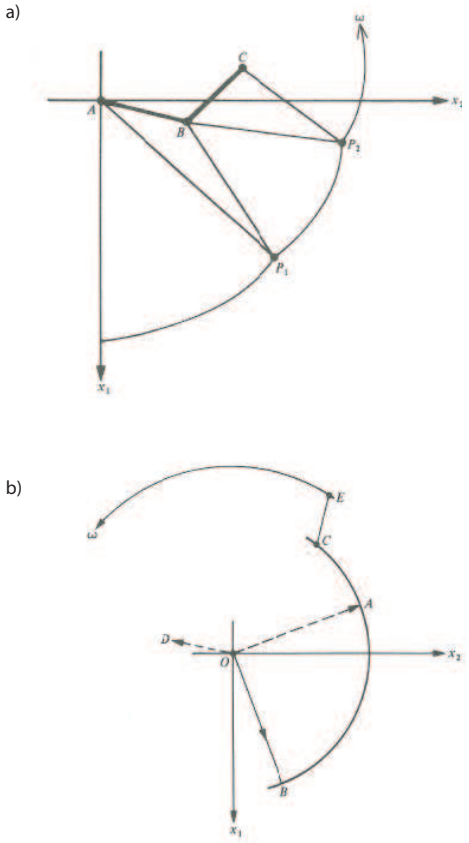

Figure 2.1: Motion of the instantaneous rotation axis ω due to a) step and b) delta excitation functions. The figure a) shows that at the time T_1, when ω is at P_1, the excitation pole is shifted from A to B; ω now turns about B with radius BP_1 until time T_2, when ω is at P_2, and a second shift in the excitation occurs from B to C. The figure b) shows that initially $\omega = 0$, $\psi = 0$. At the time T_1 a delta function excitation occurs and for a short time displaces ψ from O to A. ω jumps to B, $\frac{\pi}{2}$ behind A in phase, and now rotate about O. At the time T_2, ω is at C and a second impulse occurs in the direction OD; now ω moves to E and continues to rotate about O but with a modified radius [Lambeck, 1980].

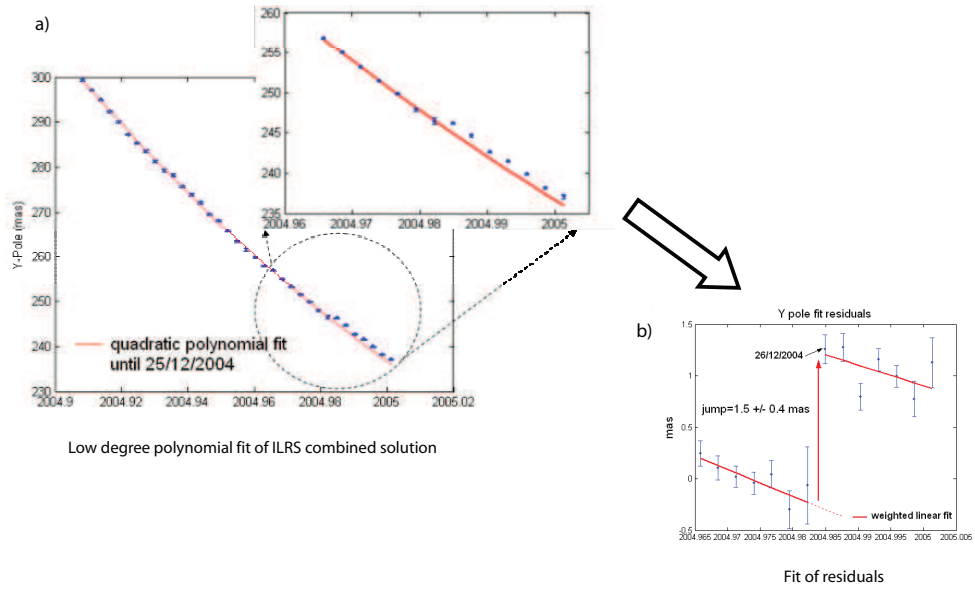

Figure 2.2: Preliminary estimates of the earthquake effect on pole motion provided by the International Laser Ranging Service (ILRS) on 19th January 2005. a) Zoom of the jump in the y-pole component data in correspondence of the Sumatra earthquake. b) Residuals of the quadratic polinomial fit of the y-pole component data in which a jump of magnitude of about $1.5 - 2.0$ mas is evidenced [Bianco et al., 2005a].

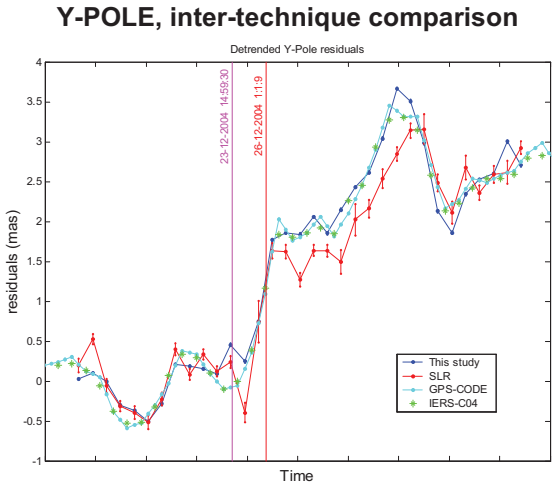

Figure 2.3: Comparison of detrended daily y-pole estimates, the red line shows SLR (combined ILRS product), the blue line represents GPS estimates obtained in the study of Bianco et al. [2005b] (see "This study" in the figure) and cyan shows the daily GPS computed at CODE (courtesy of U. Hugentobler). The green asterisks refer to the official IERS C04 solution. The independent solutions give a coherent measure of the Y-pole displacement during the Great Sumatra event [Bianco et al., 2005b].

	Lon (deg)	Lat (deg)	Width (km)	Length (km)	Strike (deg)	Rake (deg)	Dip (deg)	Slip (meter)	Depth (km)
S01	94.610	2.375			300			5	
S02	93.902	2.918			315			15	
S03	93.359	3.625			330			15	
S04	93.018	4.449			345			15	
S05	92.823	5.326			350			15	
S06	92.667	6.212			350			15	
S07	92.435	7.077	200	100	340	90	11	15	2
S08	92.165	7.934			345			15	
S09	91.970	8.811			350			15	
S10	91.853	9.702			355			15	
S11	91.853	10.598			5			15	
S12	91.970	11.488			10			15	
S13	92.165	12.366			15			5	

Figure 2.4: Seismic fault geometry.

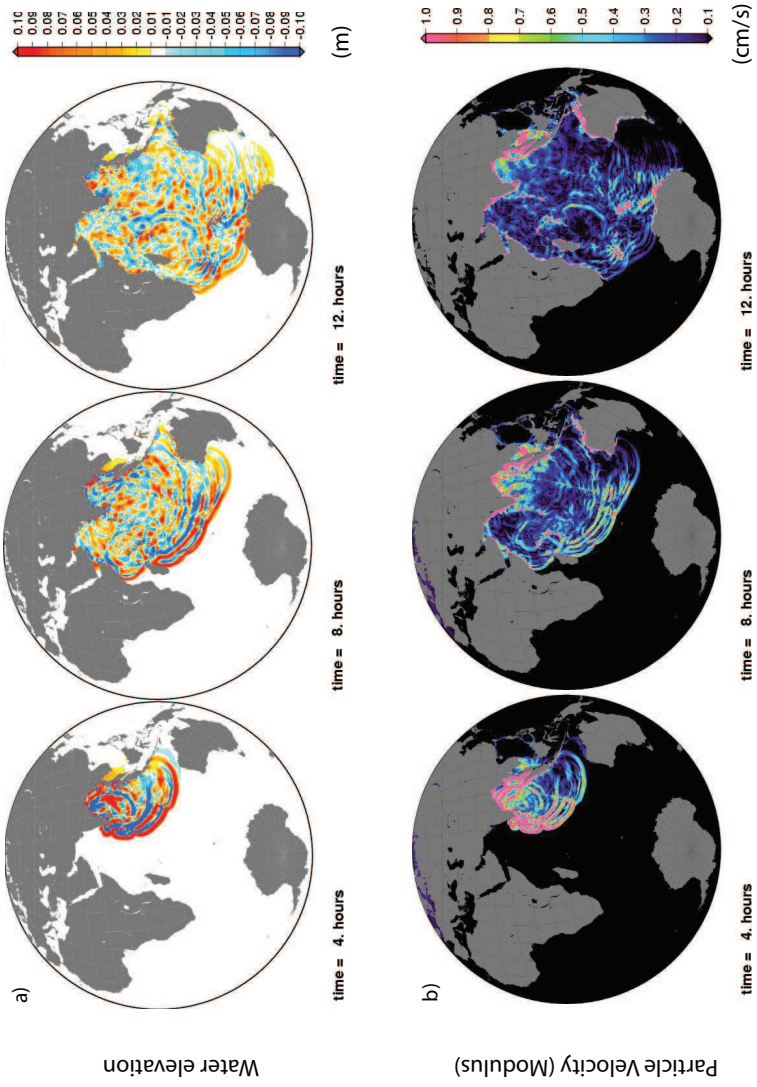

Figure 2.5: Snapshots of the propagating tsunami taken at 4 hours interval show a) the water elevation, b) the modulus of the horizontal velocity field. In the snapshots a) the red area show an elevation greater than 10 cm. In the in the snapshots b) the pink area evidence a velocity greater than 1 cm/s (36×10^{-3} km/h)

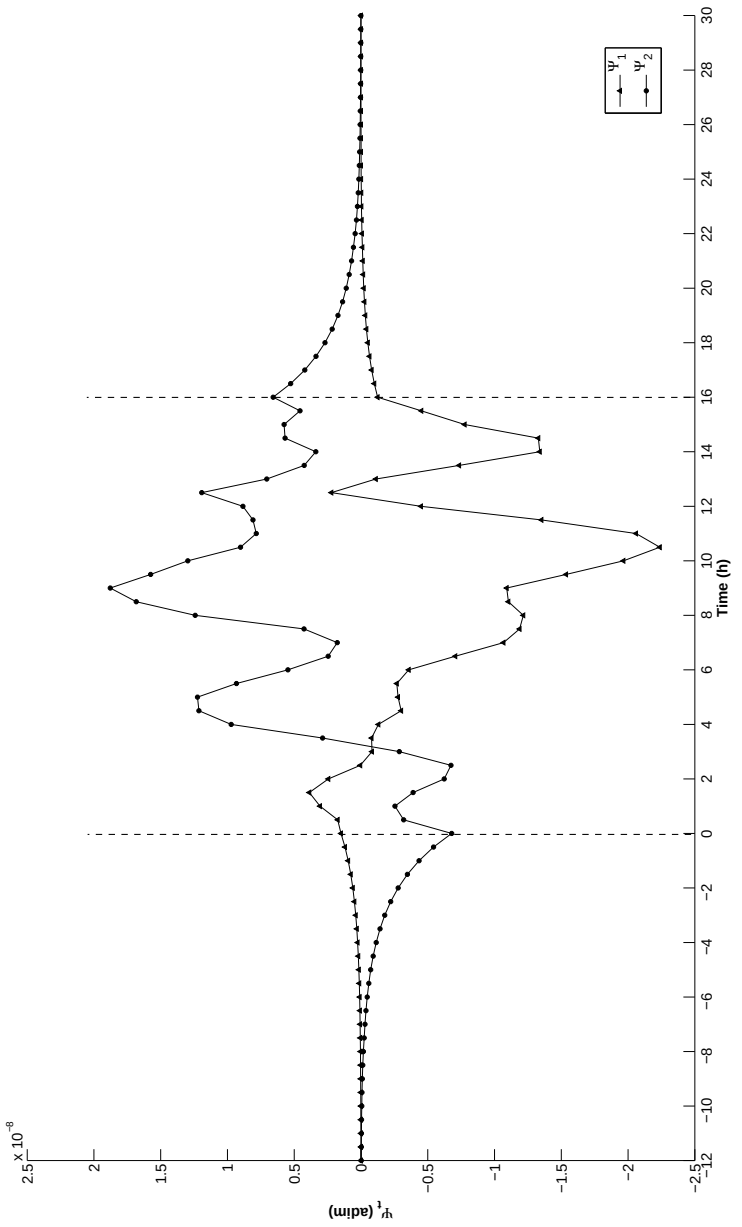

Figure 2.6: Temporal evolution of Ψ_1 and Ψ_2 components of the total excitation function.

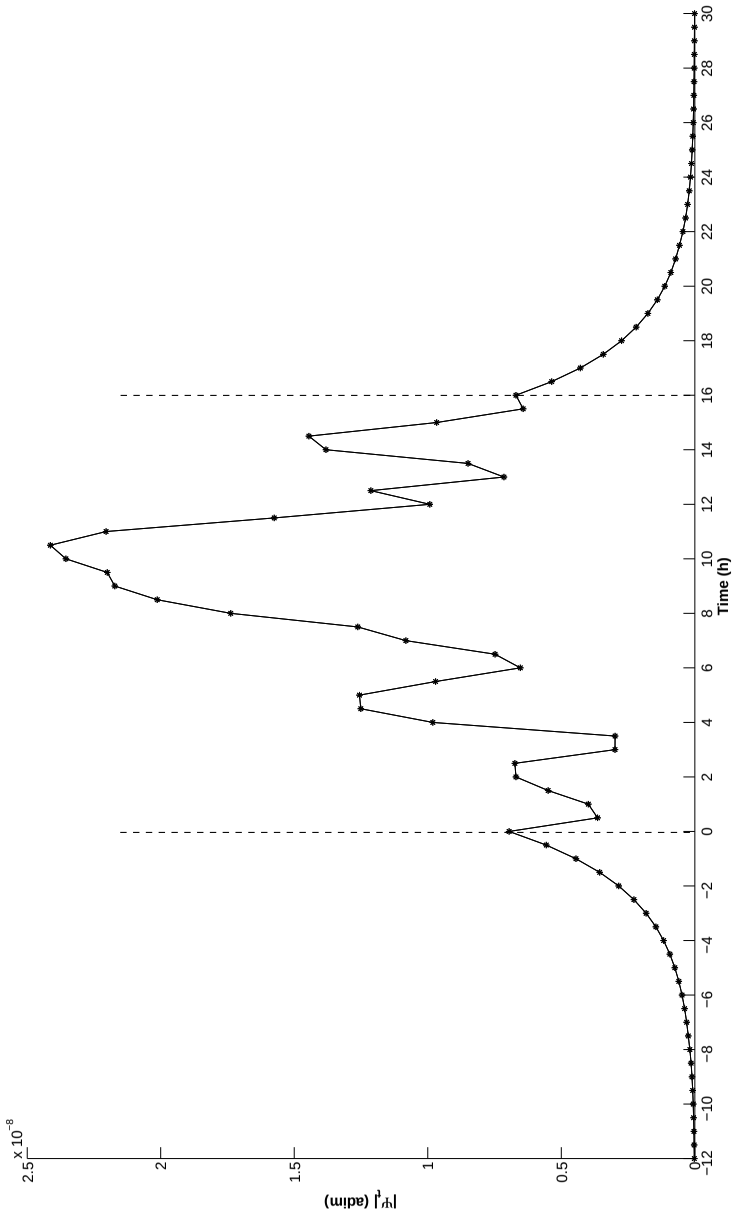

Figure 2.7: Temporal evolution of $|\mathbf{\Psi}_t|$.

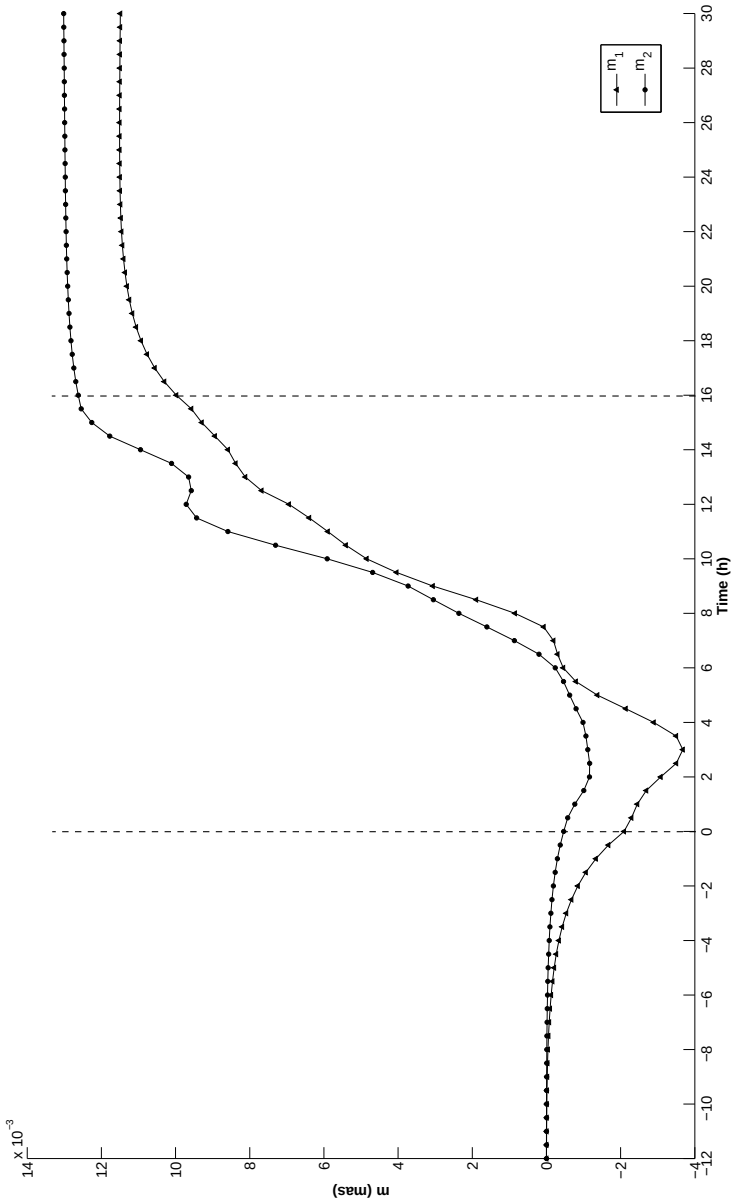

Figure 2.8: Temporal evolution of m_1 and m_2 components of the instantaneous pole of rotation.

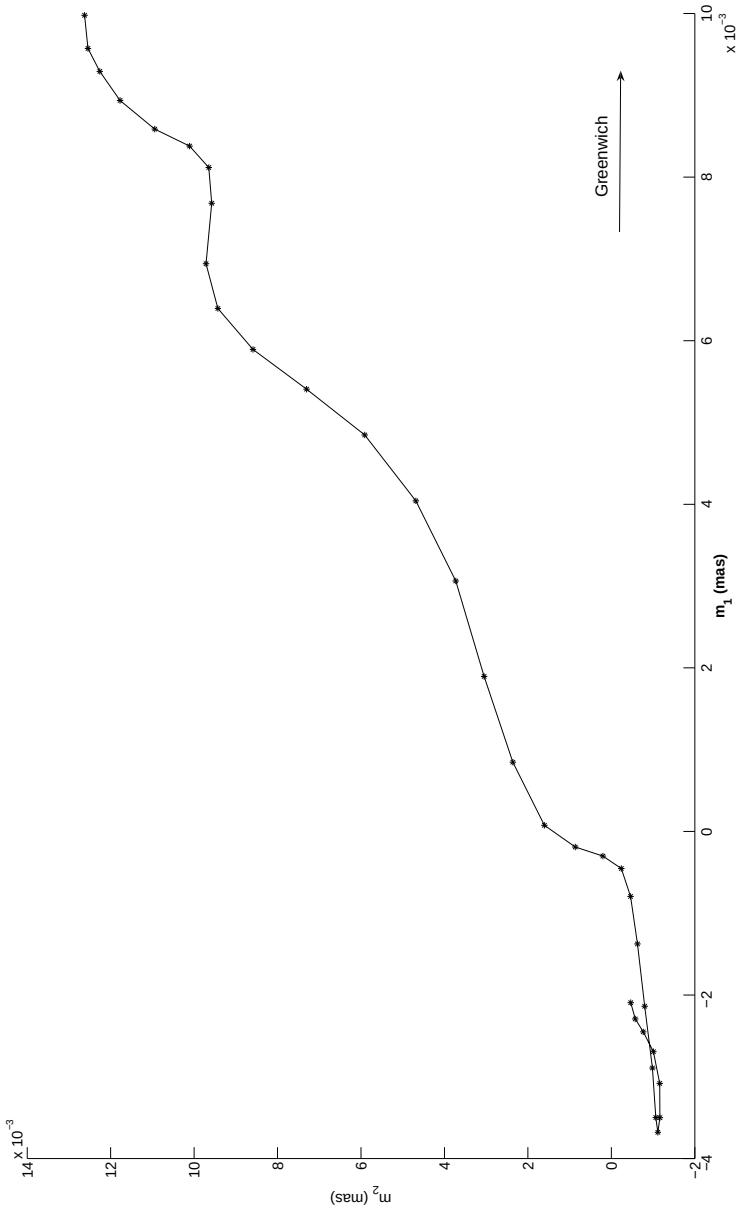

Figure 2.9: Polar motion during the 16 hours of the tsunami propagation.

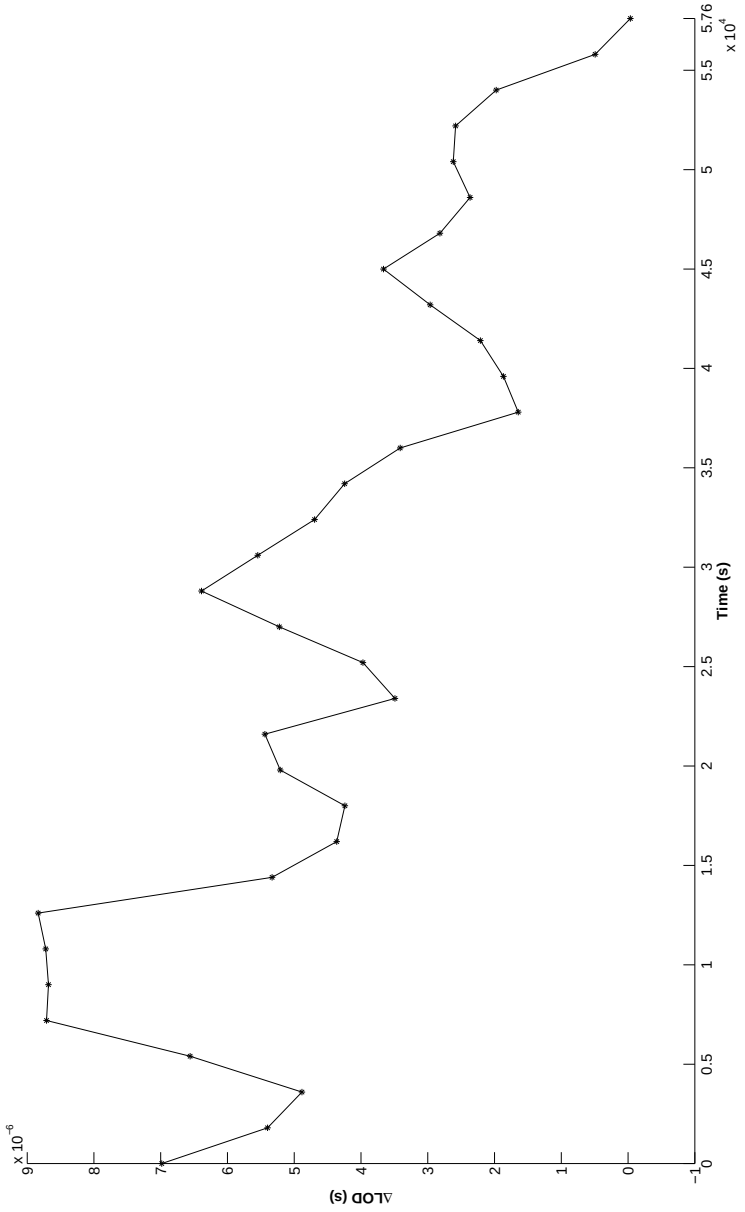

Figure 2.10: LOD variation during the 16 hours of propagation of the simulated tsunami.

Chapter 3

Coseismic and postseismic stress diffusion associated with the Sumatra earthquake

3.1 Introduction

The giant Sumatra earthquake occurred on December 26^{th}, 2004 perturbed the stress field configuration over a large area surrounding the event source, triggering a seismic sequence consisting of 2992 aftershocks recorded just in the first three months, and 4643 aftershocks recorded in the first six months.

When an earthquake occurs the Earth reacts elastically and is instantaneously deformed. This deformation, which is referred to as "static" or "coseismic", induces an instantaneous change of the state of stress in the surrounding lithosphere [Boschi and Dragoni, 2000, Casarotti et al., 2001, Casarotti and Piersanti, 2003].

Due to their long term fluid behaviour, the astenosphere and the mantle react to the imposed elastic shear stress deforming and superimposing a time-dependent deformation process on the elastic static coseismic contribution; this phenomenon is referred to as postseismic deformation. [Ranalli, 1995, Casarotti et al., 2001, Casarotti and Piersanti, 2003].

The earlier studies of the stress transfer by large earthquakes and their interaction with seismogenetic structures at global scale is due to Romanowicz [1993], who examined the spatio-temporal pattern of energy release by great strike-slip and thrust earthquakes in a time window from 1908 to 1992, evidencing alternating periods of these mechanisms. While the fault interactions at local or regional scale are supported by phenomenological and modelistic evidences and is now considered an important feature in the seismic hazard assessment [Stein, 1999, Parsons et al., 2000, Steacy et al., 2005], the idea of remote triggering of earthquakes and of fault interaction at great distances is still a controversed topic [Kerr, 1998]. A quantitative approach to the interaction between earthquakes at great distances was addressed for the first time by Pollitz et al. [1998], who analyzed the spatio-temporal correlation between the viscoelastic relaxation process following the great Alaska earthquakes of the 1950s and 1960s and the following seismic activity of the north-east Pacific. Subsequently other studies about the fault interactions at global scale were carried out in the works of Marzocchi [2000], Melini et al. [2002], Casarotti et al. [2001], Casarotti and Piersanti [2003]

In this chapter we discuss an analysis of the coseismic (static) and postseismic (quasi-static) stress diffusion due to the December 26^{th}, 2004 Sumatra earthquake along the Sunda-Java Trench, following both an analytical and

a numerical approach. In order to evaluate the stress changes due to the Sumatra earthquake we computed the Coulomb stress on the source mechanisms of Sumatra aftershocks taken both from the Centroid Moment Tensor (CMT) and United States Geological Survey (USGS) catalogues in a time window spanning two years (from December 26^{th}, 2004 to November 30^{th}, 2006), that includes Nias (March 28^{th}, 2005, $M_w = 8.6$) and Java (July 17^{th}, 2006, $M_w = 7.7$) earthquakes, and analyzed the spatio-temporal stress pattern. The modeling approach and the dataset selection used to perform this analysis, will be explained in the subsections 3.2.1 and 3.2.2 respectively.

In the subsection 3.2.3 we briefly outline the theoretical principles of the analytical, viscoelastic spherical model of global postseismic deformation (PSD) originally proposed by Piersanti et al. [1995, 1997] and of the numerical finite-element (FE) package FEMSA developed by Volpe et al. [2007], which have been used to calculate the stress field components.

The results obtained with the two modeling approach have been resumed in section 3.3 where we give a detailed description of the results obtained in the modeling and we make a more deeper analysis, focusing on the Java earthquake, in order to validate our modeling procedures.

3.2 Modeling approach

3.2.1 The Coulomb Failure Function

Earthquakes occur when the shear stresses which act to rupture a fault are large enough to overcome the normal (or clamping) stresses that, in combi-

nation with friction, prevent a locked fault from slipping [Freed, 2005]. This balance is conveniently expressed by the *CoulombFailureFunction* (CFF), that is a useful tool to evaluate the interactions between the perturbation to the stress field due to earthquakes and the preexisting seismogenic structures [Stein, 1999]. The Coulomb stress σ_c, or Coulomb Failure Function CFF, is given by [Stein, 1999, Cocco and Rice, 2002]

$$\sigma_c = CFF = \tau + \eta(\sigma_n + p) \tag{3.1}$$

where τ is the shear stress (i.e. parallel to the slip direction), σ_n is the normal stress (by convention assumed positive if the fault is unclamped), p is the pore fluid pressure and η is the friction coefficient.

Equation (3.1) represents the balance between the shear stress τ that acts to break and the normal stress σ_n that tends to clamp the fault. The term $(\sigma_n + p)$ is the effective normal stress and takes into account the pore fluid pressure that acts against the normal stress by reducing the resistance to shear fracture and the resistance to sliding ([Ranalli, 1995] and references therein).

Since is not possible to know the absolute value of stress on a fault, we can calculate the Coulomb stress changes caused by an earthquake by means of changes in the shear and normal stresses, by using the expression

$$\Delta\sigma_c = \Delta CFF = \Delta\tau + \eta(\Delta\sigma_n + \Delta p) \tag{3.2}$$

The knowledge of the sign of the CFF variations on a fault allows us to predict if the stress field imposed by an earthquake acts to promote (ΔCFF>0) or

to oppose (ΔCFF<0) the rupture of the fault.

The calculation of the ΔCFF is indipendent from any knowledge of the prevailing regional stresses or any preexisting stress fields from other events [Freed, 2005].

Pore fluid pressure changes are commonly assumed to be proportional to normal stress changes and included into an effective coefficient of friction, η', so that eq. (3.2) is written in the following form [Cocco and Rice, 2002]

$$\Delta CFF = \Delta\tau + \eta'\Delta\sigma_n \tag{3.3}$$

where the effective coefficient of friction is defined as:

$$\eta' = \eta(1 - B) \tag{3.4}$$

where B is Skempton's coefficient, which by means of laboratory experiments typically ranges between 0.5 and 0.9 [Roeloffs, 1996]. The effective coefficient of friction varies in a range from 0.0 to 0.75, with an average value of $\eta' = 0.4$ that is often used ([Cocco and Rice, 2002] and reference therein).

3.2.2 Dataset selection

In order to evaluate the CFF variations we have to project the Coulomb stress over the seismic rupture planes of the events we are going to study. To this aim we selected a sequence of aftershocks of the Sumatra earthquake taken from the CMT and USGS catalogues in the time window from December 26^{th}, 2004 to November 30^{th}, 2006 located in the geographical area included between longitudes 85°E and 115°E and latitudes -15°N and 20°N.

In the selected period we collected 7219 events at all magnitude values from the USGS catalogue. Since the USGS catalogue does not provide a focal mechanism solution, we assigned to the selected events the same focal mechanism of the mainshock, i.e. that of the "composite" source evaluated in the work of Tsai et al. [2005], which is located at at (6.6°N, 93.0°E) at depth of 25 km with strike, dip and rake angles respectively of 343.0°, 6.1°, 107.0° (figure 3.1).

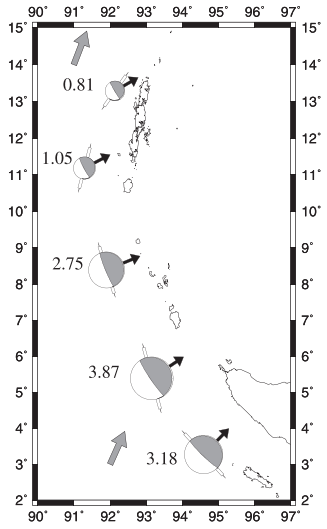

Table 2. Source Parameters for the Final, Five-Source Model[a]

Source	Strike	Dip	Rake	Moment	M_W	ε
I	318	6.4	94	0.318	8.94	0.00
II	345	6.3	109	0.387	9.00	0.00
III	343	5.8	95	0.275	8.90	0.02
IV	15	8.4	132	0.105	8.62	0.04
V	35	8.1	155	0.081	8.54	0.01
Comp	343	6.1	107	1.15	9.31	0.02

[a]Strike, dip and rake are given in degrees. Moment is given in units of 10^{30} dyne-cm. ε describes the relative size of the non-double-couple component of the moment tensor and is calculated as $-e_2/\max(|e_1|, |e_3|)$ where e_i are the ordered eigenvectors of the moment tensor. Values for a composite ("Comp") solution obtained by summing the moment-tensor components of the individual sources are also listed. The centroid location and time for the composite source are 6.6°N, 93.0°E and 214 s.

Figure 3.1: Multiple CMT solution obtained by [Tsai et al., 2005] for the Sumatra earthquake with their focal parameters. In yellow the "composite" source.

For the 875 CMT aftershocks instead, the strike, dip and rake angles of the two nodal planes are provided for each event [Dziewonski et al., 2000]. However, we had to discriminate the actual fault plane between the two solutions to project the Coulomb stress and calculate the CFF variation. To this aim we followed the idea developed in the work of Casarotti et al. [2001] in which the authors evaluated the stress transferred by eight particular big earthquakes, selected from 1960 to 1989, to all the seismogenic structures of the circum-Pacific area. At this purpose at first they divided the circum-Pacific area into smaller areas enclosing plate boundary segments of roughly coherent geometry and fault type mechanism, then selected a great number of events from the CMT catalogue and evaluated their actual focal mechanism, on which project the Coulomb stress, on the basis of a functional relashionship among the strike, dip and rake angles of the first and second nodal plane for all the earthquakes occurring within these areas [Casarotti et al., 2001].

According to the procedure adopted in Casarotti et al. [2001], in figure 3.2 we plotted the two CMT focal solutions on the (rake, dip), (dip, strike) and (rake, strike) planes, and looked for a functional relashionship of the focal angles. The first and second nodal planes are plotted in black and red, respectively.

From the 875 CMT solutions, we selected a set of 299 events having mainly thrust type mechanism (black ellipse in figure 3.2c), i.e. with rake$>0°$ and dip$<45°$, as expected along a subduction zone; this set also has strike angles greater than 270°, quite in agreement with the north-eastward subduction direction of the Australia plate boundary.

The red ellipse in figure 3.2c encloses the complementary nodal planes of the events enclosed in the black one; these solutions have strike directions between 120° and 180° and dip>45°, which are not compatible with the subducting direction of the Australia plate. Since the investigated area has predominantly a thrust-type regime, we selected as actual fault planes those in the black ellipse and discarded those included in the red one.

Another interesting cluster, including 152 events, is evidenced in 3.2c in the blue ellipse. For this set we could not follow the selection procedure adopted before because the corresponding cluster of their complentary nodal planes are distributed on the whole (rake, strike) plane without forming a cluster; therefore the solutions evidenced in the blue ellipse were selected without any discrimination procedure.

We will refer to the 451 events enclosed in the black and blue ellipses as the group a.

For the remaining 424 CMT events, the selection of their actual nodal planes has been carried out by isolating small groups of events whose focal mechanisms have the following features:

- compatibility with the regional tectonic regime, such as thrust-type fault mechanism;
- similarity of the focal mechanism with the nearest source of the five mechanisms obtained by Tsai et al. [2005];
- direction of strike angle following the path of the subduction zone boundary;

- similarity of the focal mechanism among small groups of events located in the same geographic area.

We will refer to these 424 events as the group *b*.

3.2.3 Modeling the stress field

Once the focal mechanisms have been selected, the next step consists of calculating the time-dependent stress components. These have been calculated using both an analytical, viscoelastic, spherical model of global postseismic deformation developed by Piersanti et al. [1995, 1997] and a finite-element method recently developed by Volpe et al. [2007]. In the next two subsections we outline the characteristics of the two methods.

The semi-analytical method

The semi-analytical model of global postseismic deformation originally developed by Piersanti et al. [1995, 1997] and further refined by Boschi et al. [2000] is based on a spherical, incompressible, layered, laterally homogeneous and self-gravitating Earth model and allows to compute the time-dependent response to a seismic excitation through a normal mode decomposition of the physical observables.

This approach is based on the correspondence principle of linear viscoelasticity [Fung, 1960] that enables us to deal with equations of motion formally identical to these of the elastic case, provided that we solve the problem in the Laplace domain and define a complex rigidity $\tilde{\mu}(s) = \frac{\mu s}{s+\frac{\mu}{\eta}}$, where η is the viscosity and s is the Laplace variable. The equations of motion of a linear

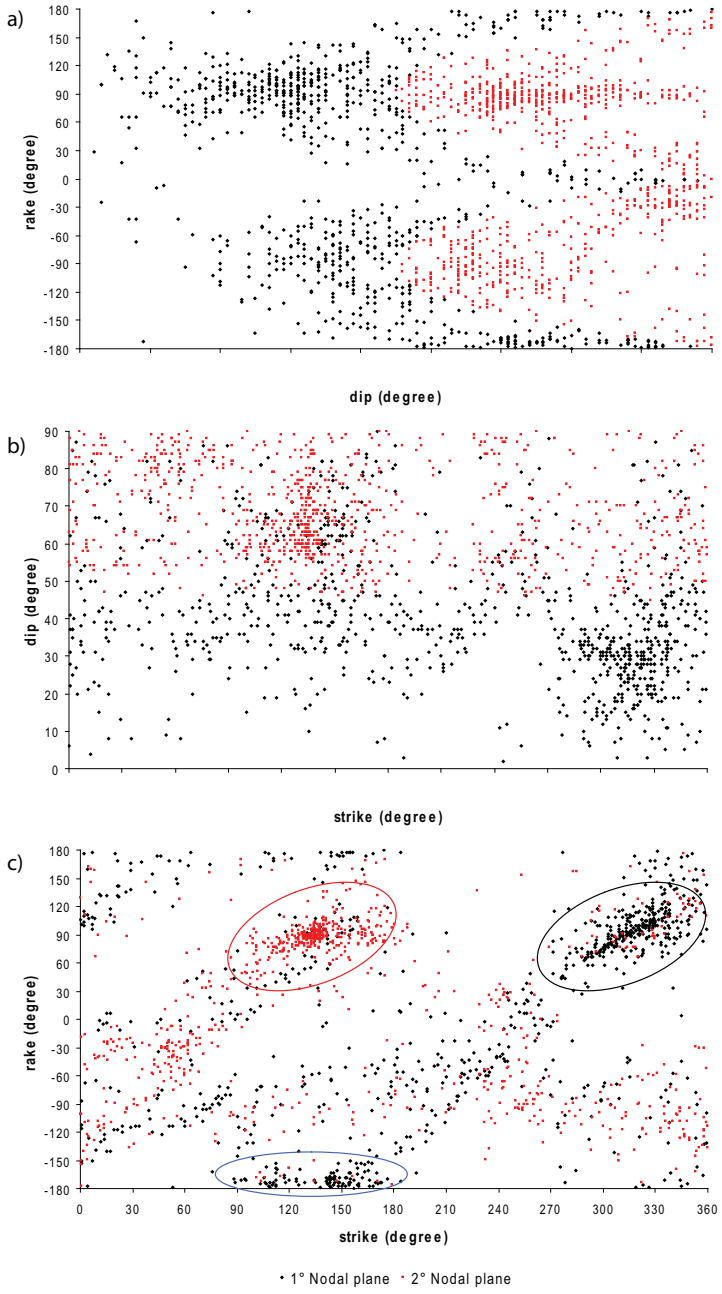

Figure 3.2: Functional relationship among parameters of the two nodal planes for all selected CMT events.

viscoeleastic Maxwell body are then written in the Laplace domain in the following form:

$$-\rho\nabla\tilde{\phi}_1 - \nabla(\tilde{\mathbf{u}}\cdot\rho_0 g_0\mathbf{e}_r) + \nabla\cdot\tilde{\mathbf{T}} = \rho\tilde{\mathbf{f}} \tag{3.5}$$

$$\nabla\cdot\tilde{\mathbf{u}} = 0 \tag{3.6}$$

$$\nabla^2\tilde{\phi}_1 = 0 \tag{3.7}$$

$$\tilde{\mathbf{T}} = 2\tilde{\mu}\tilde{\mathbf{E}} + \tilde{\mathbf{p}_1}\mathbf{I} \tag{3.8}$$

$$\tilde{\mathbf{E}} = \frac{1}{2}[\nabla\cdot\tilde{\mathbf{u}} + (\nabla\cdot\tilde{\mathbf{u}})^T] \tag{3.9}$$

where the tilde denotes Laplace-transformed variables and the subscrtipts 0 and 1 denote the equilibrium and the perturbed quantities [Peltier, 1974, Wu and Peltier, 1982, Sabadini et al., 1984, Wolf, 1991, Spada, 1992, Piersanti et al., 1995]. Equation (3.5) states the momentum conservation and $\tilde{\mathbf{f}}$ represents the equivalent force distribution corresponding to a point seismic dislocation [Smylie and Mansinha, 1971, Mansinha et al., 1979, Piersanti et al., 1995], whereas $\tilde{\mathbf{u}}$ and $\tilde{\mathbf{T}}$ represent the displacement field and the stress tensor. Equation (3.6) is the incompressibility condition; equation (3.7) is the Poisson equation for the incremental gravitational potential $\tilde{\phi}_1$; equation (3.8) is the costitutive law of an incompressible viscoelastic medium with linear rheology, where $\tilde{p}_1$ is the incremental pressure and $\mathbf{I}$ is the identity matrix. Equation (3.9) is the definition of tensor of the infinitesimal deformations $\tilde{\mathbf{E}}$.

The solution of the problem is obtained through a decomposition of the physical quantities on a spherical harmonic basis and applying symmetry

constraints. In this way the equation system (3.5) - (3.9) is linearized and for each harmonic degree and order it is possible to obtain a sets of first-order ordinary differential equations, for the poloidal and toroidal parts [Smylie and Mansinha, 1971, Piersanti et al., 1995]:

$$\frac{d}{dr}\,\mathbf{y}_l^m = \mathbf{S}^l\,\mathbf{y}_l^m + \mathbf{f}_l^m \tag{3.10}$$

$$\frac{d}{dr}\,\mathbf{z}_l^m = \mathbf{T}^l\,\mathbf{z}_l^m + \mathbf{g}_l^m \tag{3.11}$$

where the poloidal six-component vector $\mathbf{y}_l^m$ and the toroidal two-component vector $\mathbf{z}_l^m$ contain harmonic expansion coefficients of displacement, incremental stress field and gravity potential. In order to simplify the notation the Laplace variable s has been left implicit. The elements of $\mathbf{S}^l$ and $\mathbf{T}^l$ depends on the mechanical and the rheological parameters of the Earth model [Piersanti et al., 1995]; the functions $\mathbf{f}_l^m$ and $\mathbf{g}_l^m$ contain the spectral components of the body force equivalent to a point dislocation [Smylie and Mansinha, 1971, Mansinha et al., 1979, Piersanti et al., 1995].

The solution of the equations (3.10) and (3.11) is obtained by imposing as boundary conditions the continuity at the internal interfaces and vanishing shear stresses at the free surface and at the Core-Mantle-Boundary [Sabadini et al., 1982]. The solution at the CMB is then propagated to the observer radius [Gilbert and Backus, 1966]. Once the solution in the Laplace domain has been obtained, the time-dependence can be recovered by applying the residue theorem [James, 1991, Spada, 1992].

Starting from the semi-analytical model the time evolution of the stress tensors can be computed by a summation of the spherical harmonic terms.

Since the harmonic expansions of displacements and stress contain rapidly oscillating terms, a special care has to be devoted to the choice of the sum truncation point to ensure its convergence. This issue has been addressed in the work of Casarotti [2003], which carried out a detailed study assuming that the solution reaches convergence at an harmonic degree depending mostly on the radial distance D between the source and the receiver (see Tab. 1.1 in Casarotti [2003]).

In our study of the postseismic stress relaxation due to the Sumatra event, we assumed a radial rheological stratification with an 80 km elastic lithosphere, a 200 km thick asthenosphere, a uniform mantle and a fluid inviscid core. Both the asthenosphere and mantle are caracterized by a viscoelestic Maxwell rheology with viscosity values of 10^{19} Pa s and 10^{21} Pa s respectively. The density and the rigidity values are obtained by volume-averaging the corresponding PREM reference values [Dziewonski and Anderson, 1981]. The seismic source for the Sumatra earthquake has been modeled with the composite point source of the work of Tsai et al. [2005] (figure 3.1). The analysis has been carried out in a time window of two years; for each aftershock the stress field has been evaluated at the exact time of its occurrence.

As explained before, a critical numerical problem is represented by the convergence of the harmonic expansion, since the number of required degrees strongly increases when the source and receiver get radially closer [Riva and Vermeersen, 2002, Casarotti, 2003]. To overcome convergence problems with aftershocks occurring at depths close to the mainshock depth, we constrained the source-receiver radial distance to assume a minimum value of 20 km. If the mainshock depth is z, we assigned at all aftershocks located at depths

between z and $z + 20$ km depth $d = z + 20$ km, while at aftershocks located between z and $z - 20$ km we assigned a depth $d = z - 20$ km. To the aftershocks located at exactly at the same depth of the mainshock we assigned alternately a depth $d = z \pm 20$.

The numerical finite-element method

FEMSA, the acronym for "Finite Element Modeling for Seismic Applications", is a numerical simulation tool aimed to calculate stress and displacement fields resulting from seismic faulting [Volpe et al., 2007]. FEMSA is based on CalculiX, a free 3D structural Finite Element solver, created by Guido Dhondt & Klaus Wittig (http://www.calculix.de/).

In order to evaluate the stress changes due to the Sumatra earthquake we considered a spherical domain consisting of a portion of spherical zone about 1000 km thick spanning 9×10^7 km^2 on the Earth surface (figure 3.3); the domain has been meshed with 38348 20-nodes brick elements resulting in a mesh containing 171537 nodes. The mesh was designed to be finer near the Sumatra source where the internode distance is about 2 km, while outside the region the spatial resolution decrease with increasing distance [Volpe et al., 2007].

The domain is laterally homogeneous and has been rheologically layered in two different ways in order to perform the coseismic and postseismic analyses. For static analysis, a multi-layered elastic rheology has been considered, while for the quasi-static analysis a three-layered model has been defined with a 125 km thick elastic lithosphere, a 250 km thick viscoelastic asthenosphere with η=10^{18} Pa s and 625 km viscoelastic mantle with η=10^{21} Pa s. Both the

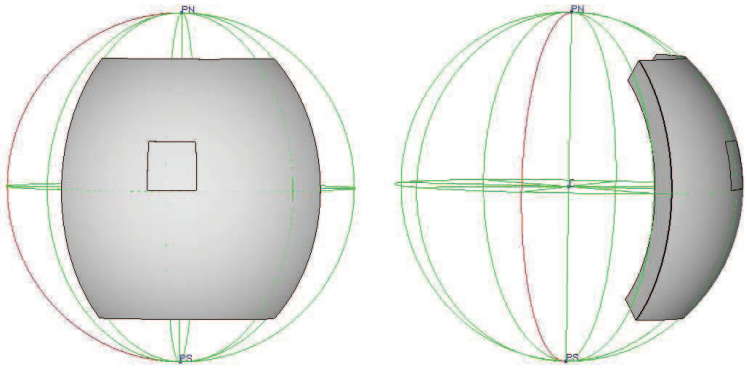

Figure 3.3: Portion of spherical zone used in the numerical simulation [Volpe et al., 2007].

asthenosphere and the mantle have a linear Maxwell viscoelastic rheology. In both analyses the elastic parameters have been evaluated by a volume average of the corresponding PREM values [Dziewonski and Anderson, 1981]. The simulation has been carried out in a time window of two years with a time step of one year, the seismic source has been modeled with the multiple point sources model proposed by Tsai et al. [2005] (figure 3.1).

Although in the FE modeling the faults are usually considered as contact interfaces, CalculiX has no contact capabilities implemented yet, so the sources are implemented by FEMSA as a distribution of double couples of forces, under the equivalent body force theorem [Volpe et al., 2007]. The application points of the double couple of forces are chosen in groups of four according to the slip vector and eventually moved in order to obtain the correct orientation accordingly with the dip angle.

For computational semplicity the simulation is carried out assuming zero strike and subsequently field values, for strike angles different from zero, are obtained by means of a suitable reference frame rotation. While the FE

simulation computes only pure strike-slip (0°, 180°) and dip-slip (90°, 270°) mechanisms, arbitrary rake angles are modeled as a linear combination of pure mechanisms.

Since the FE method is intrinsically limited to deal with finite domains, careful boundary conditions have to be introduced, in order to avoid edge effects [Wolf, 2004]. FEMSA implements the so-called Okada inhomogeneous boundary conditions. Since the Okada model [Okada, 1985, 1992] provide the exact analytical solution for the displacement field generated by a faulting source within an infinite homogeneous domain, the exact displacements (in an assumed infinite domain) belonging to nodes on the bottom and lateral surfaces delimiting the volume can be calculated and imposed as inhomogeneous boundary conditions [Volpe et al., 2007].

The postseismic stresses have been calculated using FEMSA in a time window of two years (i.e. from December 2004 to December 2006) with a time step of one year. In order to associate the most reliable stress values to all the aftershocks in the sequence, we applied a coseismic stress to the aftershocks occurred in the time window from December 26^{th}, 2004 to the June 30^{th}, 2005 (6 months); a postseismic stress evaluated after one year from the mainshock to the events occurred from July 1^{st}, 2005 to the June 30^{th}, 2006 and finally a postseismic stress evaluated after two years to the aftershocks occurred from July 1^{st}, 2006 to the November 30^{th}, 2006. This procedure is schematically represented in figure 3.4.

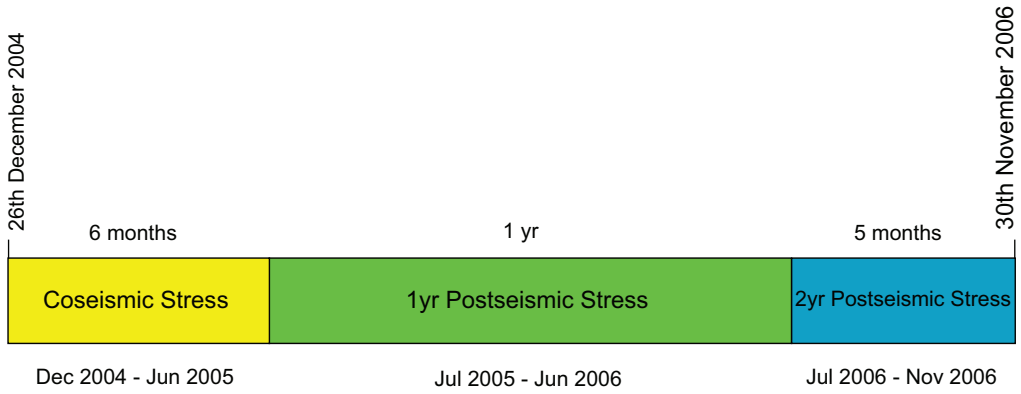

Figure 3.4: Diagram which represents the time step used for the postseismic numerical finite-element simulation.

3.3 Results and discussions

3.3.1 CFF sign variations distribution

Figures 3.5a and 3.5b show the coseismic CFF variation in the investigated area at a depth of 20 km above and below the mainshock, respectively. The Coulomb stress has been projected on a plane with the same orientation of the mainshock fault. The plots evidence that both at depth of 5 km and of 45 km (i.e. $\pm$20 km from the Sumatra hypocentre), a wide area around the source is interested by an overall CFF variation of about 0.2 bar (black rectangles in figures 3.5a and 3.5b). Along the Sunda arc, at depth of 5 km (figure 3.5a), the ΔCFF$>$0 and $\sim$0.02 bar; while at depth of 20 km below the mainshock, the stress changes are less effective (figure 3.5b).

Figures 3.6a and 3.6b represent the postseismic CFF sign variations on the aftershocks of the Sumatra event for the USGS and CMT datasets, respectively, computed with the semi-analytical method.

As we described in subsection 3.2.2, for the USGS events we projected the Coulomb stress on the focal mechanism of the mainshock, while for the CMTs we selected the focal mechanisms as explained in subsection 3.2.2. Nevertheless, the plots of figures 3.6a and 3.6b evidence a similar pattern of the CFF variations for both datasets, even if the sample of the selected earthquakes from the two catalogues is quite different.

The plots in figures 3.6 show that for the aftershocks located above the equator there is no predominant regime of ΔCFF sign. The ΔCFF value of Nias 2005 earthquake obtained by projecting the Coulomb stress on the focal mechanism of the Sumatra mainshock, is very low (5×10^{-3} bar), while it is negative (-4×10^{-4} bar) using the CMT focal mechanism, obtained in the selection of the group *a* (subsection 3.2.2). In the region, below the equator, there is a prevalent regime of ΔCFF<0, as if the Sumatra earthquake would not act to promote the ruptures; more to on south, in correspondence of the 2006 Java earthquake (green star), there is a cluster of events occurring in ΔCFF>0 conditions.

As described in subsection 3.2.3, the simulations with the semi-analytical model have been carried out with a constraint on the radial distance between the source and the receiver in order to prevent convergence problems in the harmonic sums. The computations performed with the finite-element method does not suffer from these restrictions and therefore have improved our modeling of stress relaxation.

The stress field obtained with the numerical simulation has been calculated by superimposing contributions of each point source obtained by Tsai et al. [2005]. For each aftershock the six stress components have been ob-

tained by finding the grid point closest to the aftershock hypocenter.

Figure 3.7 shows the coseismic CFF sign variations obtained both in the coseismic and in the postseismic case by means of the finite-element method.

Figure 3.7a shows the sign of the coseismic CFF variations projected on the USGS events. In the northern part of the investigated region (above the equator), as obtained with the analytical model (figure 3.6), the plots do not show a prevalence of positive or negative CFF variations. Below the equator, instead, there is a striking prevalence of earthquakes occurring in conditions of positive CFF variation; this result has a great statistical relevance because there are almost no earthquakes with negative ΔCFF sign in the southern part.

In figure 3.7b we represented the coseismic CFF sign variations on the CMT earthquakes. Even if in this case the statistical significance is weaker with respect to that obtained with the USGS catalogue, due to the smaller sample of events, the pattern of the ΔCFF sign distribution confirms what observed in the previous plots, except for the presence of a cluster of earthquakes, located in the southern-eastern part of the investigated region, interested by a general negative CFF variation (green circle).

Figure 3.8 shows the postseismic CFF sign variations both for the two catalogues obtained with the FE method. If we compare postseismic sign variations (figures 3.8a and 3.8b) with the coseismic ones (figures 3.7a and 3.7b), we observe that they have qualitatively the same pattern. In correspondence of the Nias earthquake source there is an increase of CFF variation of about 1 bar for both datasets. The ΔCFF value of the Nias event is the same both in coseismic and postseismic case because, as we explained in the

subsection 3.2.3 (figure 3.4), we associated a coseismic stress to the events belonging to the first six months after the Sumatra earthquake. More to the south, in correspondence of the Java event, occurred in July 17^{th}, 2006 the values in the postseismic case are three times greater (i.e. 7×10^{-3} for the USGSs and $4.5\times10^{-3}$for the CMTs) than those obtained in the coseismic. Due to the similarity of the coseismic and postseismic stress patterns, from this analysis we can conclude that the postseismic stress did not cause a change of the ΔCFF signs in the majority of the events.

In figure 3.9 we analyzed the spatio-temporal evolution of the postseismic CFF variations obtained with the finite-element method. We observe a migration of seismicity, from the equator towards the southern part of the investigated region, during the two years in which the analysis has been carried out. This pattern of seismicity is in agreement with the results obtained by Pollitz et al. [2006], who evaluated the stress changes associated with coseismic and postseismic deformation following the Sumatra and Nias events. Their results show a stress increase slowly moving towards the southern part of the Sunda arc in a time window of ten years; such increase of stress along the arc could affect the 1797 and 1833 rupture zones [Sieh et al., 2004, Pollitz et al., 2006] triggering other large earthquakes.

3.3.2 The Java earthquake

In this section our aim is to study the CFF sign variations on the cluster of events, located in the southern-eastern region along the Sunda (Java) Trench, that includes the July 17^{th}, 2006 Java earthquake (green circle in figure 3.7b).

The Java earthquake occurred off the southwestern coast of Java, Indonesia, and caused a three-meter-high tsunami which struck the southern Indonesian coasts of Java. The event is characterized by a scalar moment $M_0 = 4.61 \times 10^{20}$ Nm, corresponding to a moment magnitude $M_w = 7.7$ as a result of thrust-faulting on the boundary between the Australia plate and the Sunda plate (strike, dip and rake angles equal to 290°, 10° and 102° respectively) [Dziewonski et al., 2000]. The rupture nucleated at (-9.25°N, 107.41°E) at 34 km depth, on the shallow part of the plate boundary, about 50 km north of the Java Trench ([Dziewonski et al., 2000], http://earthquake.usgs.gov).

In the previous analyses (subsection 3.3.1) we evaluated the effect of the stress acting on this region as a consequence of the Sumatra earthquake, by projecting the Coulomb stress over the focal mechanisms selected in the subsection 3.2.2 and collected in the group *b*. The majority of the events of the cluster have a focal mechanism belonging to the group *b* (section 3.2.2) except the Java mainshock and two other seismic events whose focal mechanism belongs to the group *a*.

As described in subsection 3.3.1 the stress variations due to the Sumatra earthquake on the cluster, computed by means of semi-analytical and the finite-element modeling, show different results. The semi-analytical modeling gives predominantly a positive CFF sign variation both for the USGS and CMT cluster events (figures 3.6a and 3.6b), while in particular the Java event shows a negative ΔCFF value both projecting stress on the mainshock and on the CMT focal mechanism; this result shows that the stress field of the Sumatra event does not seem to be responsible of the rupture of the Java fault.

Both the coseismic and the postseismic stress analyses performed with the finite-element modeling on the cluster show a net presence of positive ΔCFF in case of the USGS events and a prevalence of negative ΔCFF in case of the CMT events (figures 3.7 and 3.8). In particular, in the coseismic and postseismic FE modeling, performed on the CMT events, the cluster is interested by a general negative CFF sign variation; while the Java earthquake occurs in regime of ΔCFF>0 both in the coseismic and postseismic analysis. But even if in the quasi-static case the value of ΔCFF is three times greater (4.5×10^{-3} bar) than the static case, in both cases the transferred stress values turn out to be not relevant.

Since the coseismic and postseismic FE analysis on the cluster showed different results for the two dataset, we want to exclude an error due to the choice of the focal mechanism of the group *b*. To this aim, we carried out a coseismic and postseismic stress analysis with the finite-element method projecting the the Coulomb stress on the focal mechanism ruled out in the selection of the group *b* (subsection 3.2.2) and then we tested the effect of that change on the ΔCFF signs. As a result we obtained again an high percentage of ΔCFF<0 both in the coseismic and postseismic case (figure 3.10). We observed that the change of the focal mechanism do not influence the sign of the ΔCFF and infered that the stress imposed by the Sumatra earthquake does not act to facilitate the failure of the cluster faults.

As a last step, since the spatio-temporal location of the cluster corresponds to the sequence of the Java aftershocks, we evaluated the stress field variations generated by the Java earthquake on the cluster events. At this purpose we performed the stress field calculation with the semi-analytical

method; we did not use the FE model because the simulation would require the creation of a new mesh, since the Java earthquake is located in a region in which our current mesh is less refined.

The focal mechanism used to project the stress tensor has been assumed equal to that of the mainshock (i.e. the July 17^{th}, 2006 Java source) for the USGS events, while for the CMT events we used the same procedure as described in subsection 3.2.2. In figure 3.11 are shown the results obtained. In the case of the USGS events the aftershocks enclosed in the cluster occur in a regime of positive ΔCFF, while in the case of the CMT events there is a predominant regime of negative ΔCFF for both nodal planes. This result is the opposite that we expected but since we cannot perform a detailed FE simulation without creating a new mesh, we may conclude that this could be a bias in modeling due to the constraints imposed on the hypocentral dephts.

3.3.3 Effect of postseismic relaxation on ΔCFF levels

The study of the CFF sign variations in the FEMSA modeling, both with the USGS and CMT datasets, produced qualitatively the same stress patterns both in the coseismic and in postseismic case (figure 3.7 and 3.8), and this seems to evidence that the postseismic relaxation does not act to change the signs of the ΔCFF. Therefore in this subsection we perform an analysis of the CFF variation levels in order to investigate if the postseismic relaxation induces some changes on the values of the ΔCFF. To this aim, we computed the difference between the postseismic and coseismic ΔCFF and plotted it on the histograms of figure 3.12. As described in subsection 3.2.3 (figure 3.4),

in the postseismic analysis on the USGS and CMT datasets we associated a coseismic stress to the events belonging to the first six months from the occurrence of the Sumatra mainshock. Therefore, for these events we could get a difference exactly equal to zero, that would introduce a bias in the central peak of the histogram. In order to avoid this effect we removed these events from the analyses.

From figure 3.12 it is evident that both for the USGSs and CMTs the number of events with a positive postseismic CFF variation is greater than of that with negative values. As evidenced from the CFF sign variations patterns of figures 3.7 and 3.8 the postseismic relaxation does not act to change the signs of the ΔCFF but acts to increase the CFF variations values as evidenced by the histograms of figure 3.12.

3.4 Conclusions

In this chapter we carried out an analysis of the coseismic and postseismic stress diffusion associated with the Sumatra earthquake both by means of a semi-analytical, model of global postseismic deformation and with a finite-element package (FEMSA). The stress changes have been projected assuming a focal mechanism identical to that of the mainshock for the whole sequence of events taken from the USGS, while for the events taken from the CMT catalogue the focal mechanisms have been conveniently selected between the two nodal planes.

The use of the two different modeling approaches is due to the constraints on hypocentral depth introduced in the semi-analytical method in which we

need to impose the aftershocks to be at a minimum radial distance of 20 km from the mainshock due to convergence issues, while with the numerical FE method we expected a more realistic picture of the stress changes pattern. In the numerical postseismic modeling, however, we had to introduce an artifact on the time discretization, as explained in the subsection 3.2.3, while for the semi-analytical model there is no such approximation.

The results obtained by means of the semi-analytical approach in the postseismic analysis of the USGS dataset, show that above the equator there is no predominant regime of ΔCFF sign. Below the equator there is a prevalence of negative ΔCFF signs, while more to south the events occurs in a regime of ΔCFF>0, expecially in correspondence of the cluster of events which include the Java earthquake. These considerations are also valid for the analysis on the CMT dataset even if they are not so evident due to the small sample of selected events from the catalogue.

The coseismic and postseismic analysis carried out by means of the numerical finite-element method showed both in the coseismic and in the postseismic case the same stress pattern. This is evident for both the examined datasets. The plots do not show a net prevalence of the positive or negative CFF variations in the region above the equator, but what is surprising is the complete absence of events occurring in regime of ΔCFF<0 in the southern part of the investigated region, below the equator. This represents quite a significant statistical result, particularly evident in the USGS dataset. The analysis performed on the CMT dataset shows the same result above the equator, but is quite different in the southern region because the cluster in correspondence of the Java earthquake shows mostly earthquakes occurring

in conditions of ΔCFF<0.

From the results of the FE modeling we obtained an high percentage of negative ΔCFF signs for the Java seismic sequence also when we projected the stress tensor on the conjugated nodal planes, both in the coseismic and in the postseismic case; therefore we inferred that this cluster does not obey to the stress regime imposed by the Sumatra event. This can be explained if we consider the large energy release of the Java earthquake ($M_w = 7.7$), that leads us to conclude that the evolution of this cluster is dominated by the stress regime imposed by the Java earthquake.

Nevertheless, the study of the stress variations due to the Java event and performed with the semi-analytical model gave again a global negative CFF variation. This is not what we were expecting, but confirms that the results obtained with this modeling are strongly affected by the constraints imposed on the hypocentral depths.

The final test that we performed is concerned with the effect of postseismic relaxation on ΔCFF levels. As described in subsection 3.3.1 the analysis of the stress diffusion, carried out with FEMSA, shows a small impact of the posteismic relaxation on the ΔCFF signs. This effect, due both to the short time scale in which the stress analysis has been performed (i.e. 2 years) and the rheology adopted, produce as a result similar patterns of the coseismic and postseismic CFF sign variations; maybe, larger variations could have been obtained introducing a transient rheology [Yuen and Peltier, 1982, Pollitz et al., 2006]. The analyses of ΔCFF levels, reported in the plots as histograms, evidenced that, even if the postseismic relaxation does not change the ΔCFF patterns, the quasi-static relaxation process acts by prevalently

increasing the ΔCFF values.

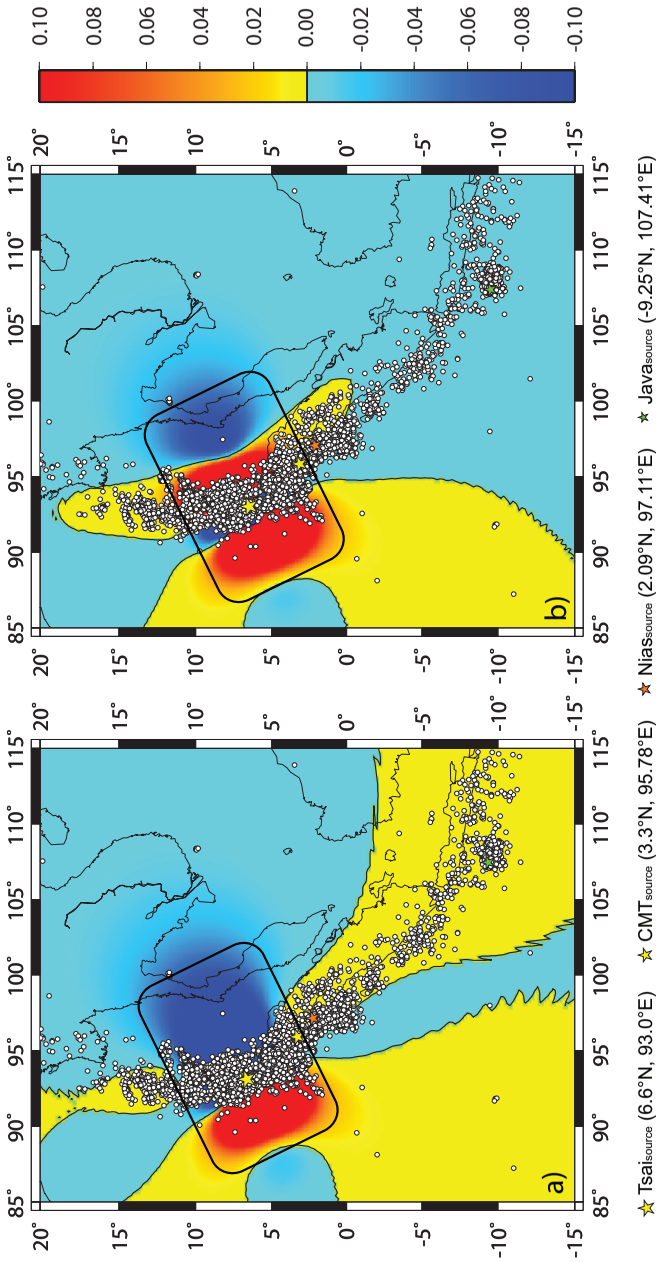

Figure 3.5: Coseismic CFF variation obtained by means of the PSD modeling at 20 km depth from the source: a) 5 km, b) 45 km. Overlapped there is the seismicity extracted from the USGS catalogue from December 26^{th}, 2004 to November 30^{th}, 2006. The black rectangle evidences the zone interested by a global CFF variation of 0.2 bar.

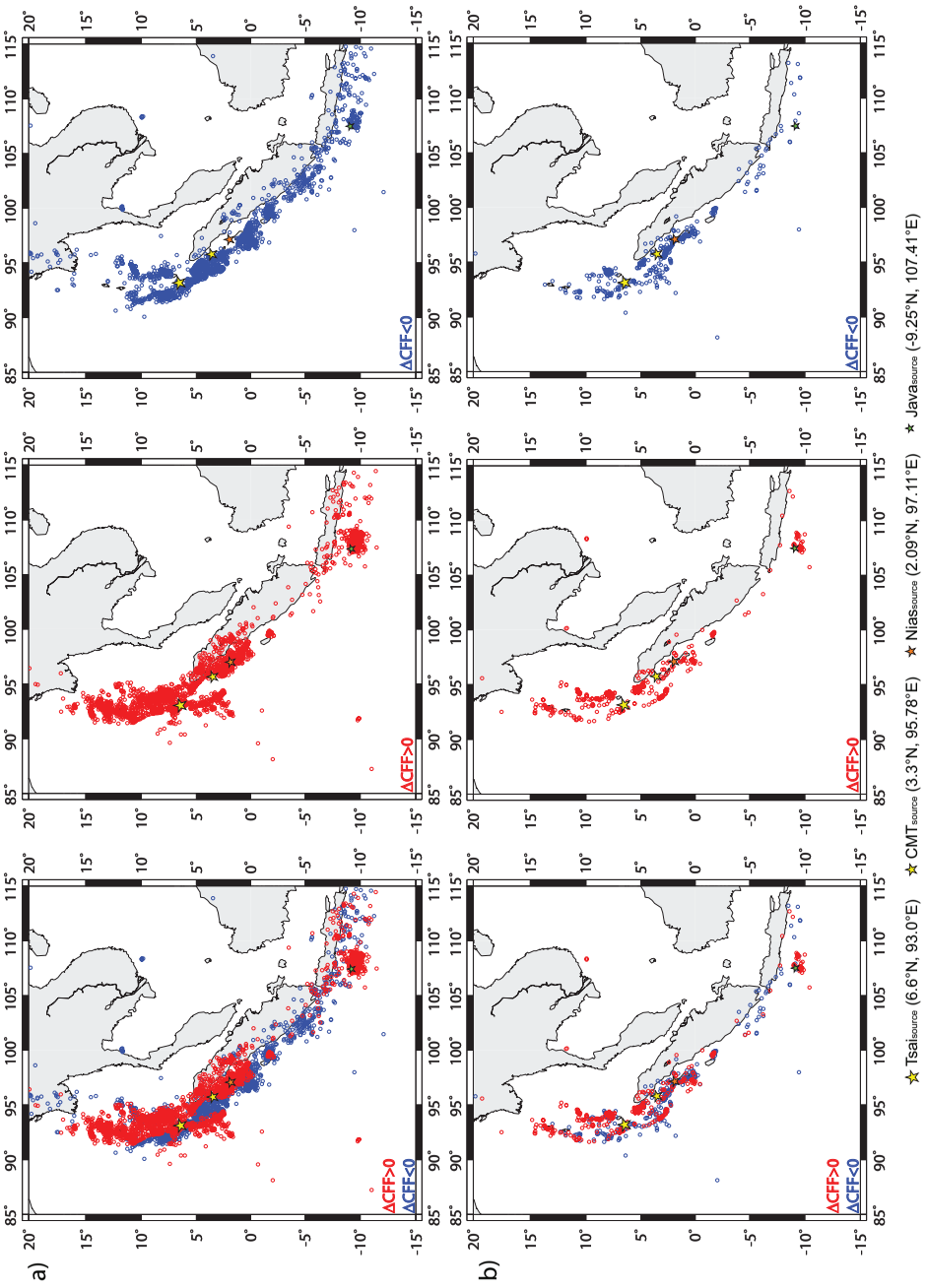

Figure 3.6: Postseismic CFF sign variations obtained by means of the PSD modeling for the a) USGS, b) CMT datasets. In the first panel positive and negative CFF variations are plotted together; the central and the right plots show positive (red) and negative (blue) ΔCFF respectively.

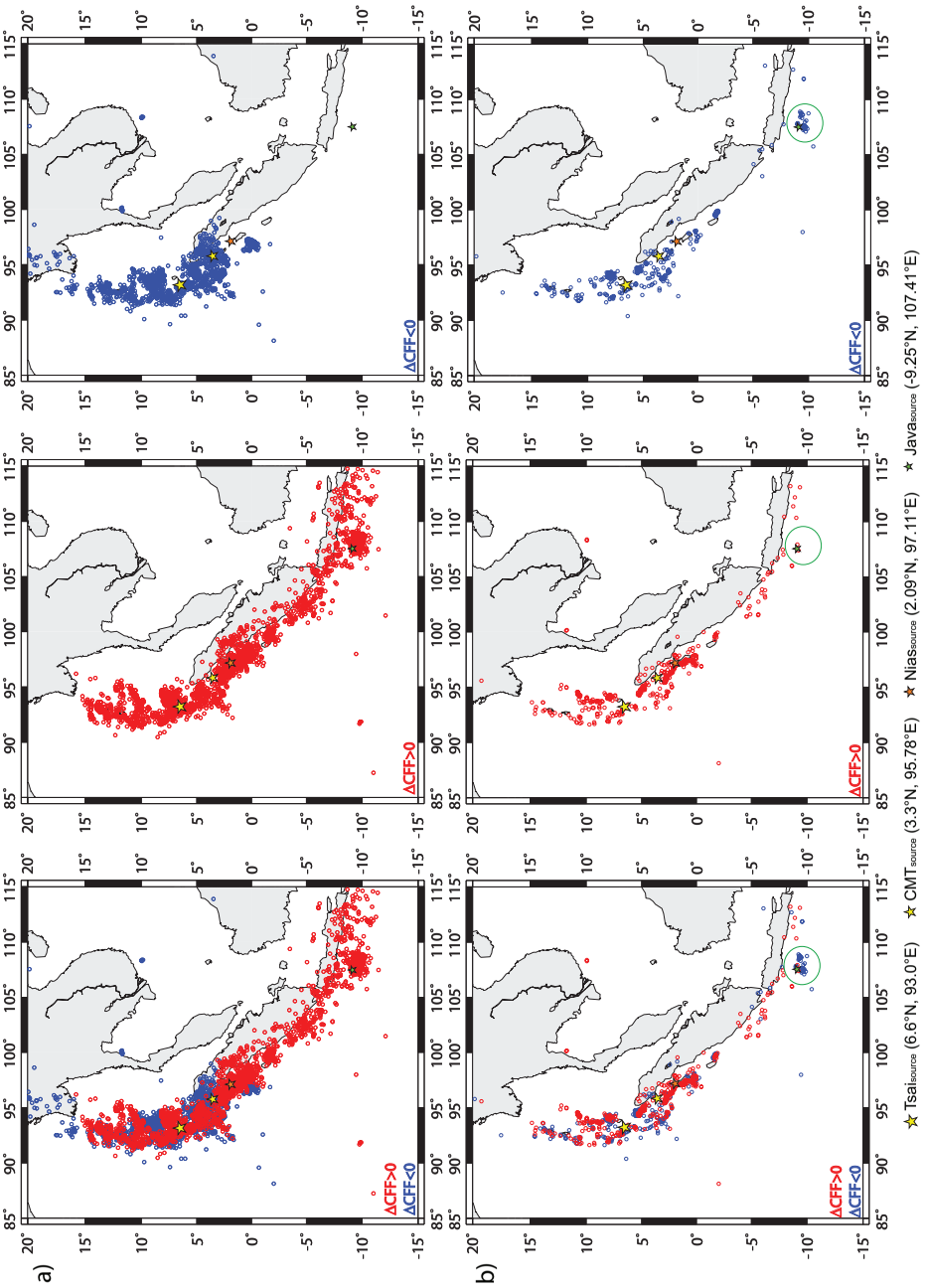

Figure 3.7: Coseismic CFF sign variations obtained by means of the FEMSA modeling for the a) USGS, b) CMT datasets. In the first panel positive and negative CFF variations are plotted together; the central and the right plots show positive (red) and negative (blue) ΔCFF respectively.

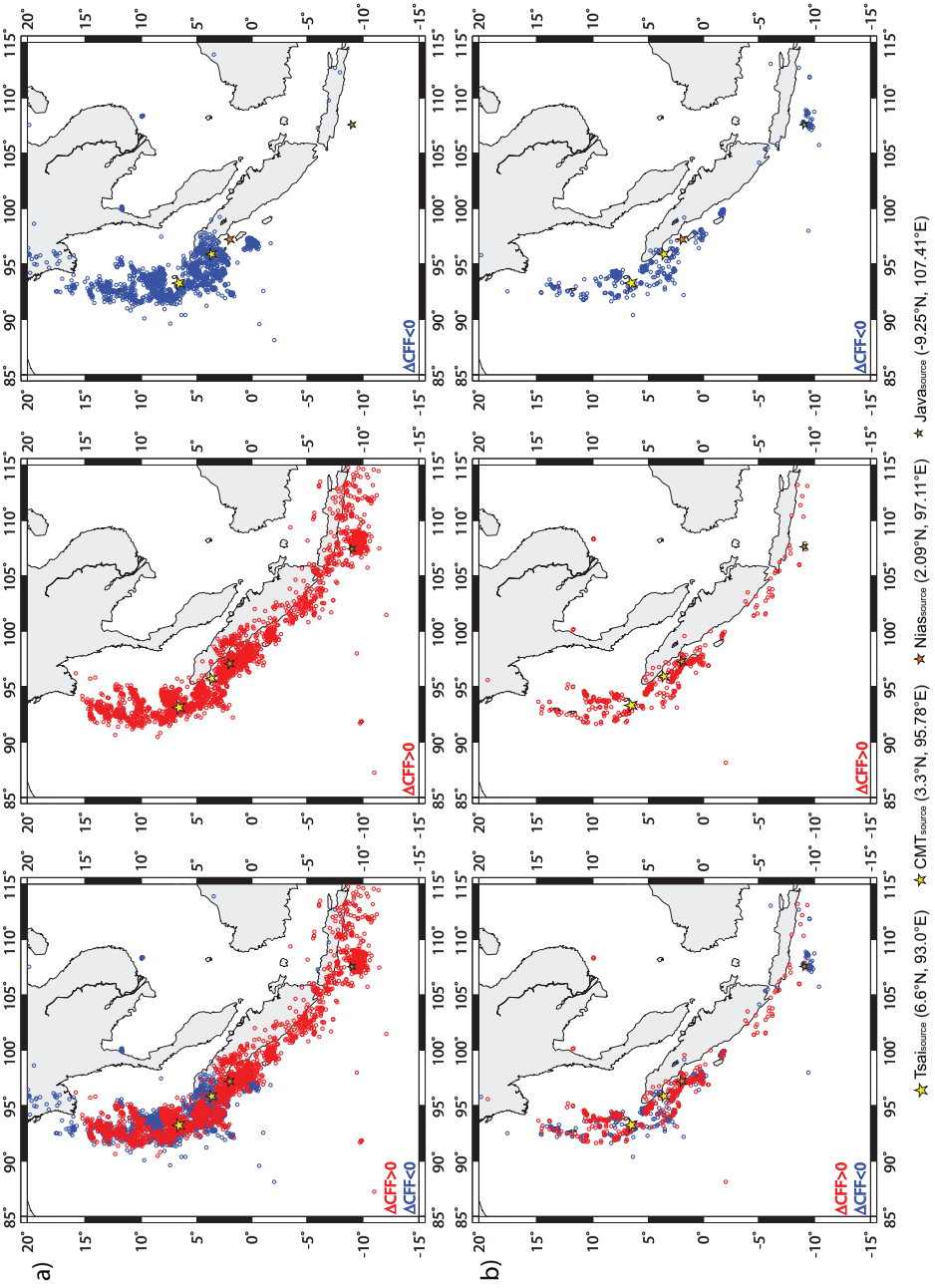

Figure 3.8: Postseismic CFF sign variations obtained by means of the FEMSA modeling for the a) USGS, b) CMT datasets. In the first panel positive and negative CFF variations are plotted together; the central and the right plots show positive (red) and negative (blue) ΔCFF respectively.

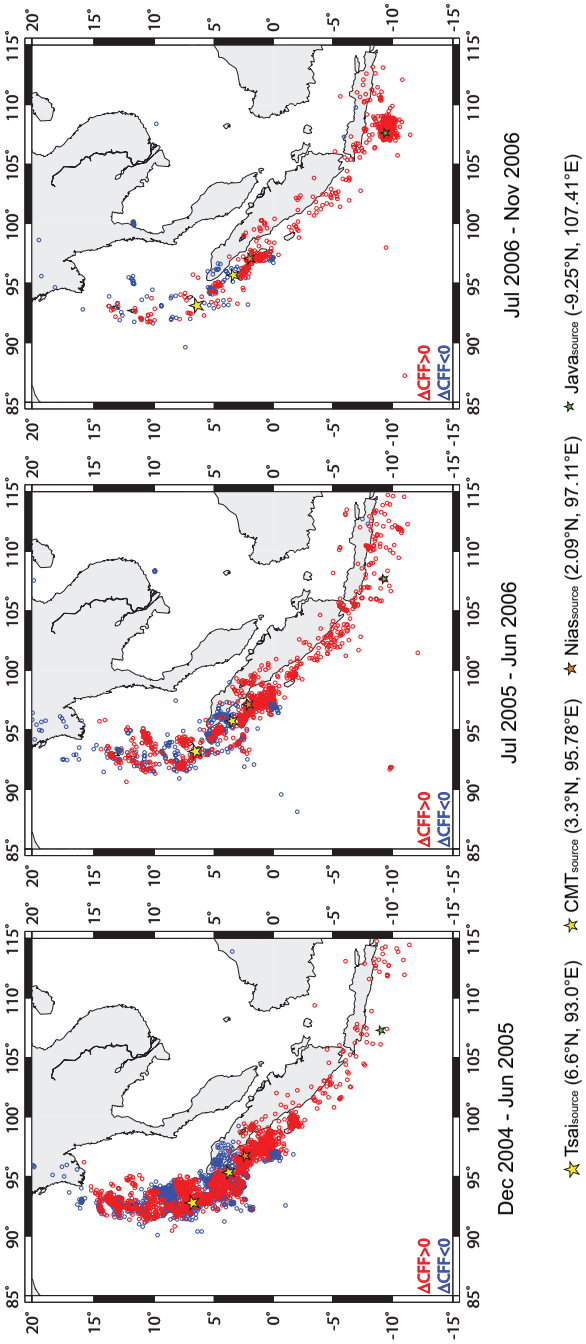

Figure 3.9: Postseismic ΔCFF evolution obtained by means of the FEMSA modeling for the USGS dataset from December 26^{th}, 2004 to November 30^{th}, 2006. The snapshot shows the results at the three time steps used for the posteseismic modeling. In the first panel positive and negative CFF variations are plotted together; the central and the right plots show positive (red) and negative (blue) ΔCFF respectively.

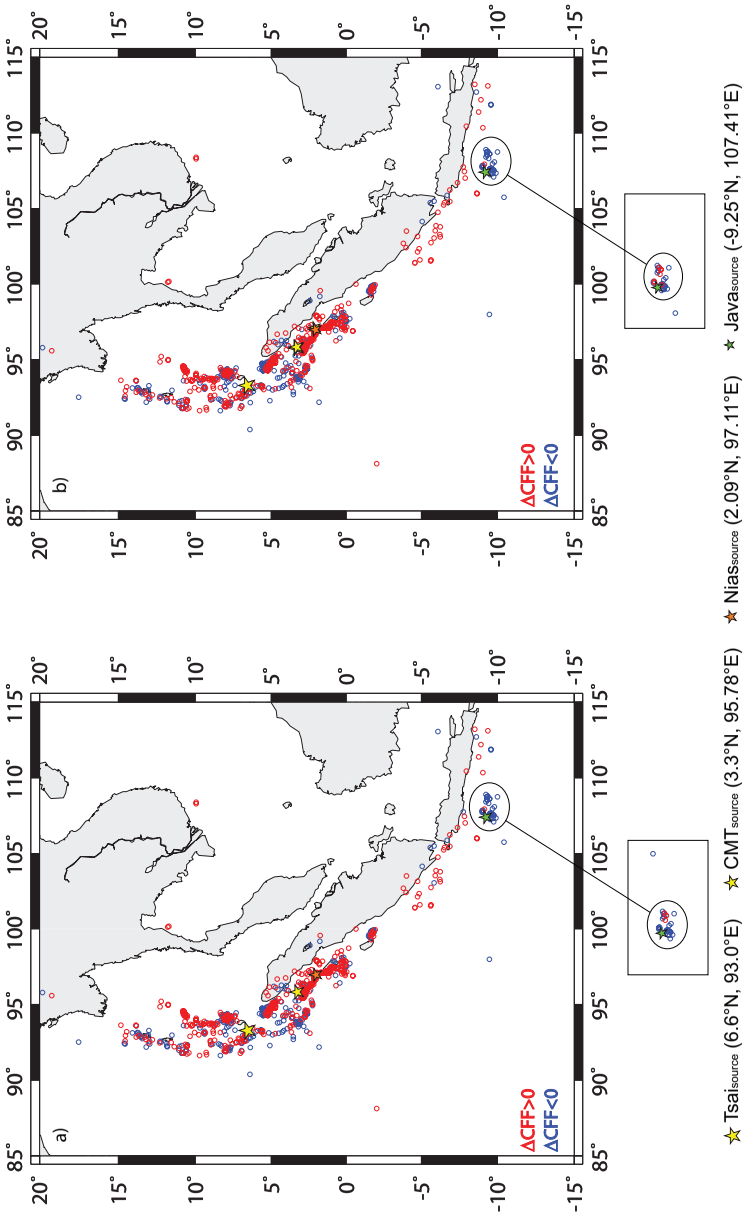

Figure 3.10: Influence of the focal mechanism changing (little box outside the figure) on the Java cluster both in the a) coseismic and b) postseismic FE modeling. In the first panel positive and negative CFF variations are plotted together; the central and the right plots show positive (red) and negative (blue) ΔCFF respectively.

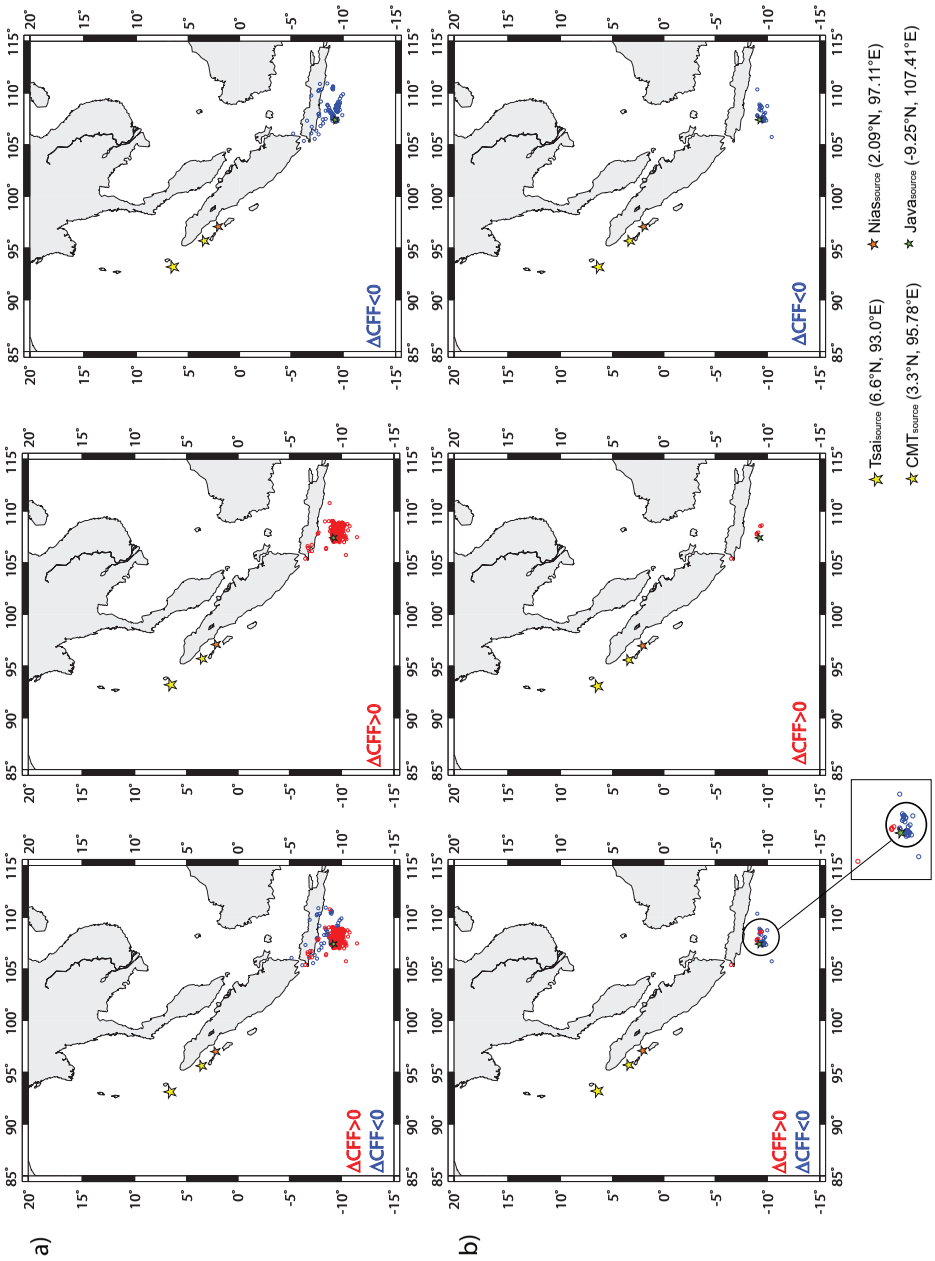

Figure 3.11: Postseismic CFF sign variations due to the stress imposed by the Java earthquake on both a) USGS and b) CMT sequence of Java aftershocks performed with the semi-analytical method. The little box outside below the figure b) is the ΔCFF sign analysis on the other CMT focal mechanism. In the first panel positive and negative CFF variations are plotted together; the central and the right plots show positive (red) and negative (blue) ΔCFF respectively.

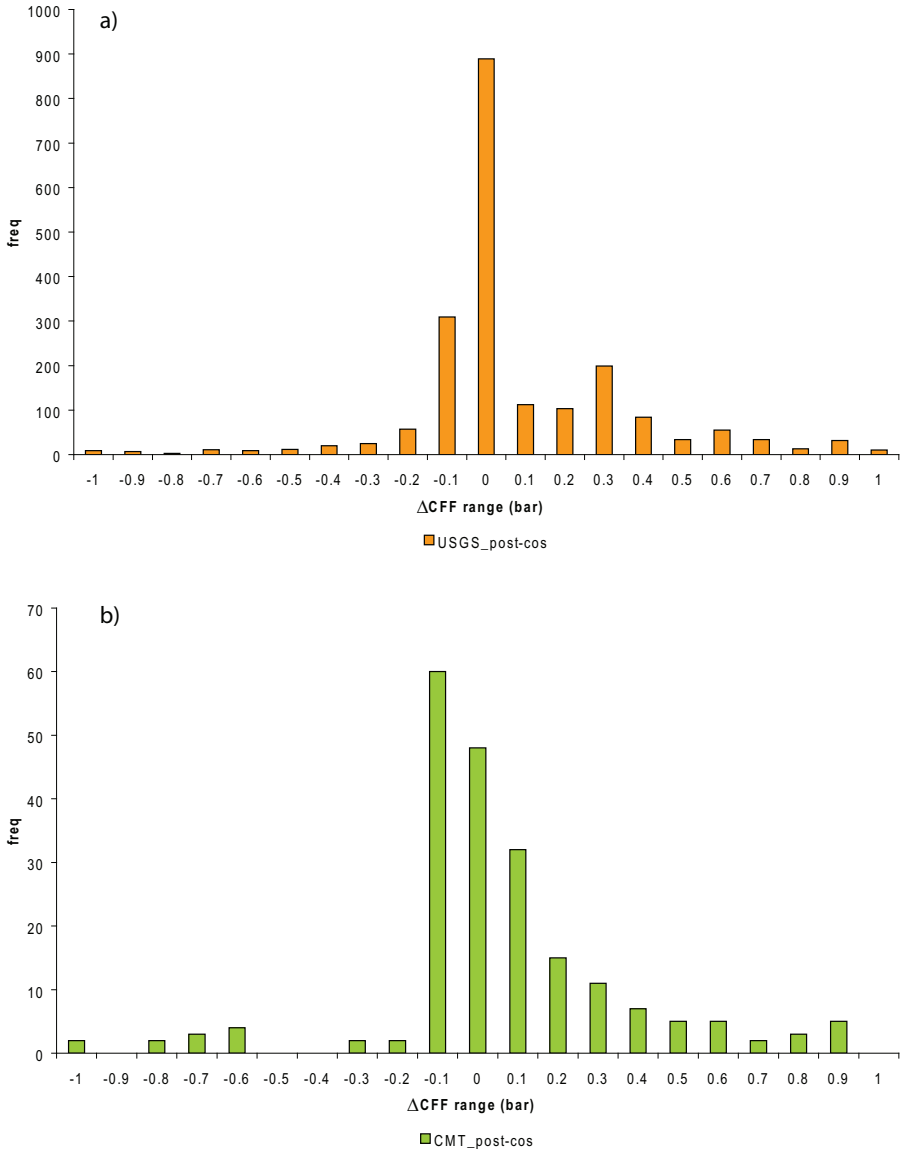

Figure 3.12: Analysis of ΔCFF levels in FEMSA modelling on the a) USGS and b) CMT events.

Chapter 4

Conclusions

The occurrence of the December 26^{th}, 2004 Sumatra earthquake has motivated this work of thesis where we have carried out a global study about the perturbations induced by the earthquake on the instantaneous rotational pole and on the LOD, and about the stress field diffusion due to the seismic rupture.

Our investigations on the Earth rotation perturbations has been motivated by the step-like discontinuity observed in the geodetic data in correspondence of the Sumatra event. Such discontinuity (not yet confirmed), turned out to be compatible with a perturbation due to a transient phenomenon such as the water mass redistribuition due to the propagation of the tsunami wave. So, following the principles of the rotational theory and by means of a numerical tsunami model, we evaluated the excitation functions which contain the perturbation and solved explicitly the instantaneous pole motion equation.

Comparing our results with the observations, our modeling produced a

negligible effect both on the perturbations to the pole path, even if qualitatively they have the same shape, and to the LOD, which results to be smaller than measurements uncertainties.

The coseismic and postseismic stress field changes have been evaluated by means of a semi-analitical, sferical model of global postseismic deformation (PSD) and a numerical finite-element method (FE). Once the stress field has been obtained, the spatio-temporal stress changes along the Sunda-Java Trench have been evaluated projecting the Coulomb stress (CFF) over the sequence of aftershocks taken from the USGS and CMT catalogues in a time window of two years from the mainshock.

The use of two distinct methods is due to the fact that the semi-analytical method is by far more efficient but limited by the constraints imposed on the hypocentral depths of the aftershocks in order to obtain the convergence of the harmonic series of the stress tensor. This means that we expect a more realistic description of the stress pattern in the numerical FE method.

The major result obtained by our analysis, on the stress imposed by the Sumatra event, is the one achieved by means of the numerical approach in the case of the USGS dataset. The pattern shows an extremely significant statistical result since all the sequence of aftershocks, below the equator, occurs in regime of ΔCFF>0. The analysis performed with the CMTs confirms the results obtained with the USGSs, even if, in this case, the sample of earthquakes is poor. We register also an exception for the CMT solution due to a cluster of events corresponding to the sequence of aftershocks following the July 17^{th}, 2006 Java earthquake, which occur in regime of ΔCFF<0.

The further analyses performed with the FE method on the cluster of the

Java earthquake, by changing the nodal plane, does not improve the results and from this we may conclude (as expected) that the stress imposed by the Sumatra earthquake does not act to promote those events that are, more likely, aftershocks of the Java earthquake.

The analyses of the postseismic viscoelastic relaxation, on the ΔCFF levels obtained with the finite-element method, evidence that the relaxation process acts by prevalently increasing the ΔCFF values.

Bibliography

L. Alfonsi, A. Piersanti, and G. Spada. Did the 1977 Sumba earthquake excite the Chandler wobble? *Earth and Planetary Science Letters*, 153: 287–292, 1997.

C. J. Ammon, C. Ji, Hong-Kie Thio, D. Robinson, S. Ni, V. Hjorleifsdottir, H. Kanamori, T. Lay, S. Das, D. Helmberger, G. Ichinose, J. Polet, and D. Wald. Rupture Process of the 2004 Sumatra-Andaman Earthquake. *Science*, 308:1133–1139, 2005. doi: 10.1126/science.1112260.

L. F. Bao, A. Piatanesi, Y. Lu, H. T. Hsu, and X. H. Zhou. Sumatra Tsunami Affects Observations by GRACE Satellites. *EOS*, 86(39):353–356, 2005.

G. Bianco, V. Luceri, and C. Sciarretta. ILRS contribution to the geophysical investigation: the December 26, 2004 earthquake effects on the terrestrial reference frame as determined by SLR observations. *http://geodaf.mt.asi.it/html_old/ilrs_0119.pdf*, 2005a.

G. Bianco, E. Boschi, R. Devoti, L. Ferraro, V. Luceri, and C. Sciarretta. Earth Axis Orientation Determined from GPS and SLR Observations during the Great Sumatra-Andaman 2004 Earthquake. *http://www-research.ge.ucl.ac.uk/COMET/Devoti_COMET05_poster.pdf*, 2005b.

E. Boschi and M. Dragoni. *Sismologia*. UTET, 2000.

E. Boschi, E. Casarotti, R. Devoti, D. Melini, A. Piersanti, G. Pietrantonio, and F. Riguzzi. Coseismic deformation induced by the Sumatra earthquake. *Journal of Geodynamics*, 42:52–62, 2006.

L. Boschi, A. Piersanti, and G. Spada. Global postseismic deformation: Deep earthquakes. *J. Geophys. Res.*, 105(1):631–652, 2000. doi: 10.1029/1999JB900278.

E. Casarotti. *Postseismic stress diffusion in a spherical viscoelastic Earth model*. Ph.D. Thesis, University of Bologna, Italy, 2003.

E. Casarotti and A. Piersanti. Postseismic stress diffusion in Chile and South Peru'. *Earth Plan. Sci. Lett.*, 206:325–333, 2003.

E. Casarotti, A. Piersanti, F. P. Lucente, and E. Boschi. Global postseismic stress diffusion and fault interaction at long distances. *Earth Plan. Sci. Lett.*, 191:75–84, 2001.

M. Cocco and J. M. Rice. Pore pressure and poroelasticity effects in Coulomb stress analysis of earthquake interactions. *J. Geophys. Res.*, 107(B2):2030, 2002. doi: 10.1029/2000JB000138.

F. A. Dahlen. The Excitation of the Chandler Wobble by Earthquakes. *Geophys. J. R. astr. Soc.*, 25:157–206, 1971.

F. A. Dahlen. A Correction to the Excitation of the Chandler Wobble by Earthquakes. *Geophys. J. R. astr. Soc.*, 32:203–217, 1973.

A. M. Dziewonski and D. L. Anderson. Preliminary reference Earth model. *Phys. Earth. Planet. Int.*, 25:297–356, 1981.

A. M. Dziewonski, G. Ekstrom, N. Maternovskaya, R. Abercrombie, M. Antolik, and M. Nettles. Centroid Moment Tensor Project, http://www.seismology.harvard.edu/projecs/CMT. 2000.

A. M. Freed. Earthquake Triggering by Satic, Dynamic, and Postseismic Stress Transfer. *Annu. Rev. of Earth and Planet. Sci.*, 33:335–368, 2005. doi: doi:10.1146/annurev.earth.33.092203.122505.

Y. C. Fung. *Fundation of Solid Mechanics*. Prentice-Hall, Englewood Cliffs, N. J., 1960.

F. Gilbert and G. Backus. Propagator matrices in elastic wave and vibration problems. *Geophysics*, 31:326–332, 1966.

R. S. Gross. The excitation of the Chandler wobble. *Geophys. Res. Lett.*, 27 (15):2329–2332, 2000.

R. S. Gross. Atmospheric and oceanic excitation of the Earths wobbles during 1980-2000. *J. Geophys. Res.*, 108(B8):2370, 2003. doi: 10.1029/2002JB002143.

R. S. Gross and B. F. Chao. The rotational and gravitational signature of the December 26, 2004 Sumatran earthquake. *Surv. Geophys*, page 18, 2006. doi: 10.1007/s10712-006-9008-1.

T. S. James. *Post-glacial deformation*. Ph.D. Thesis, Department of Geological and Geophysical Sciences, Princeton, NJ, 1991.

R. A. Kerr. Can great quakes extend their reach? *Science*, 2880:1194–1195, 1998.

H. Lamb. *Hydrodynamics*. Cambridge Univ. Press, 1932.

K. Lambeck. *The Earth's variable rotation: geophysical causes and consequences*. Cambridge Univ. Press, London, 1980.

B. Lautrup. Tsunami physics. *Kvant http://www.nbi.dk/∼lautrup/continuum/tidbits/tsunami.english.pdf*, 2005.

T. Lay, H. Kanamori, C. J. Ammon, M. Nettles, S. N. Ward, R. C. Aster, S. L. Beck, S. L. Bilek, M. R. Brudzinski, R. Butler, H. R. DeShon, Göran Ekström, K. Satake, and S. Sipkin. The Great Sumatra-Andaman Earthquake of 26 December 2004. *Science*, 308:1127–1133, 2005. doi: 10.1126/science.1112250.

C. L. Mader. *Numerical modelling of water waves*. CRC Press LLC, 2004.

L. Mansinha, D. Smylie, and C. H. Chapman. Seismic excitation of chandler wobble revisited. *Geophys. J. R. Astron. Soc.*, 59:1–17, 1979.

W. Marzocchi. Phenomenological evidence in favour of remote triggering of volcanic and seismic events. *17th Course of the International School of Geophysics: "Fault interaction by stress transfer: new horizons for understanding earthquake occurrence"*, 2000.

C. C. Mei. *The applied dynamics of ocean surface waves*. Wiley, New York, 1983.

D. Melini, E. Casarotti, A. Piersanti, and E. Boschi. New insights on long distance fault interaction. *Earth and Planetary Science Letters*, 204:363–372, 2002.

W. H. Munk and G. J. F. MacDonald. *The Rotation of the Earth.* Cambridge University Press, 1960.

Y. Okada. Surface deformation due to shear and tensile faults in a half-space. *Bull. Seism. Soc. Am.*, 75:1135–1154, 1985.

Y. Okada. Surface deformation due to shear and tensile faults in a half-space. *Bull. Seism. Soc. Am.*, 82:1018–1040, 1992.

J. Park, Teh-Ru Alex Song, J. Tromp, E. Okal, S. Stein, G. Roult, E. Clevede, G. Laske, H. Kanamori, P. Davis, J. Berger, C. Braitenberg, M. Van Camp, Xiange Lei, H. Sun, H. Xu, and S. Rosat. Earths Free Oscillations Excited by the 26 December 2004 Sumatra-Andaman Earthquake. *Science*, 308: 1139–1144, 2005. doi: 10.1126/science.1112305.

T. Parsons, S. Toda, R. S. Stein, A. Barka, and J. H. Dieterich. Heightened odds of large earthquakes near Istanbul: An interaction-based probability calculation. *Science*, 288:661–665, 2000. doi: 0.

W. R. Peltier. The impulse response of a maxwell earth. *Rev. Geophys.*, 12: 649–669, 1974.

A. Piatanesi and S. Tinti. A revision of the 1693 eastern Sicily earthquake and tsunami. *J. Geophys. Res.*, 103(B2):2749–2758, 1998.

A. Piersanti, G. Spada, R. Sabadini, and M. Bonafede. Global postseismic deformation. *Geophys. J. Int.*, 120(3):544–566, 1995.

A. Piersanti, G. Spada, and R. Sabadini. Global postseismic rebound of a viscoelastic Earth; theory for finite faults and application to the 1964 Alaska earthquake. *J. Geophys. Res.*, 102(B1):477–492, 1997. doi: 10.1029/96JB01909.

F. F. Pollitz and I. S. Sacks. Stress triggering of the 1999 Hector Mine earthquake by transient deformation following the 1992 Landers earthquake. *Bull. Seismol. Soc. Am.*, 92:1487–1496, 2002.

F. F. Pollitz, R. Bürgmann, and B. Romanowicz. Viscosity of oceanic asthenosphere inferred from remote triggering of earthquakes. *Science*, 280: 1245–1249, 1998.

F. F. Pollitz, P. Banerjee, R. Bürgmann, M. Hashimoto, and N. Choosakul. Stress changes along the Sunda trench following the 26 December 2004 Sumatra-Andaman and 28 March 2005 Nias earthquake. *Geophys. Res. Lett.*, 33:L06309, 2006. doi: 10.1029/2005GL024558.

G. Ranalli. *Rheology of the Earth.* Chapman and Hall, New York, 1995.

R. E. M. Riva and L. L. A. Vermeersen. Approximation method for high-degree harmonics in normal mode modelling. *Geophys. J. Int.*, 151:309–313, 2002.

E. Roeloffs. Poroelastic techniques in the study of earthquake-related hydrological phenomena. *Adv. Geophys*, 37:135–195, 1996.

B. Romanowicz. Spatiotemporal patterns in the energy release of great earthquakes. *Science*, 260:1923–1926, 1993.

R. Sabadini, D. A. Yuen, and E. Boschi. Polar wander and the forced responses of a rotating, multilayered, viscoelastic planet. *J. Geophys. Res.*, 87:2885–2903, 1982.

R. Sabadini, A. D. Yuen, and E. Boschi. The effects of post-seismic motions on the moment of inertia of a stratified viscoelastic Earth with an asthenosphere. *Geophys. J. R. Astron. Soc.*, 79:727–746, 1984.

K. Sieh, D. H. Natawidjaja, M. Chlieh, G. Galetzka, J.-P. Avouac, B. Suwargadi, and R. L. Edwards. The giant subduction earthquakes of 1797 and 1833, west Sumatra: Characteristic couplets, uncharacteristic slip. *Eos Trans. AGU*, 85(47), 2004. Fall Meet. Suppl., Abstract T12B-04.

W. H. F. Smith and T. Sandwell. Global sea floor topography from satellite altimetry and ship depth sounding. *Science*, 277:1956–1962, 1997.

D. Smylie and L. Mansinha. The elasticity theory of dislocations in real eart models and changes in the rotation of the earth. *Geophys. J. R. Astron. Soc.*, 23:329–354, 1971.

G. Soldati, L. Boschi, A. Piersanti, and G. Spada. The effect of global seismicity on the polar motion of a viscoelastic Earth. *J. Geophys. Res.*, 106(B4):6761–6767, 2001.

G. Spada. *Rebound post-glaciale e dinamica rotazionale di un pianeta viscoelastico stratificato*. Ph.D. Thesis, University of Bologna, Italy, 1992.

S. Steacy, J. Gomberg, and M. Cocco. Introduction to special section: Stress transfer, earthquake triggering, and time-dependent seismic hazard. *J. Geophys. Res.*, 110(B05S01), 2005. doi: 10.1029/2005JB003692.

R. S. Stein. Earthquake Conversations. *Scientific American*, 288:72–79, 2003.

R. S. Stein. The role of stress transfer in earthquake occurrence. *Nature*, 402:605–609, 1999.

R. S. Stein and E. Okal. Speed and size of the Sumatra earthquake. *Nature*, 434:581–582, 2005.

V. C. Tsai, M. Nettles, G. Ekström, and A. M. Dziewonski. Multiple CMT source analysis of the 2004 Sumatra earthquake. *Geophys. Res. Lett.*, 32: L17304, 2005. doi: doi:10.1029/2005GL023813.

M. Volpe, D. Melini, and A. Piersanti. FEMSA: A finite element simulation tool for quasi-static seismic deformation modeling. *Annals of Geophysics*, 50(3):367, 2007.

D. Wolf. Viscoelastodynamics of a stratified, compressible planet: incremental field equations and short- and long-time asymptotoes. *Geophys. J. Int.*, 104:401–417, 1991.

D. Wolf. Using commercial finite element packages for the study of earth deformations, sea levels and the state of stress. *Geophys. J. Int.*, 158(2): 401–408, 2004.

P. Wu and W. R. Peltier. Viscous gravitational relaxation. *Geophys. J. R. Astron. Soc.*, 70:435–485, 1982.

D. A. Yuen and W. R. Peltier. Normal modes of the viscoelastic earth. *Geophys. J. R. Astron. Soc.*, 69:495–526, 1982.